Computers and Mathematics with Applications 166 (2024) 51–64

Contents lists available at ScienceDirect

Computers and Mathematics with Applications

journal homepage: www.elsevier.com/locate/camwa

A low-cost, penalty parameter-free, and pressure-robust enriched Galerkin method for the Stokes equations

Seulip Lee *, Lin Mu

Department of Mathematics, University of Georgia, Athens, 30602, GA, United States

ARTICLE INFO

Keywords:
Enriched Galerkin finite element methods
Viscous Stokes equations
Interior penalty methods
Weak derivatives
Penalty parameter-free
Pressure-robust

ABSTRACT

This paper proposes a low-cost, penalty parameter-free, and pressure-robust Stokes solver based on the enriched Galerkin (EG) method with a discontinuous velocity enrichment function. The EG method employs the interior penalty discontinuous Galerkin (IPDG) formulation to weakly impose the continuity of the velocity function. However, despite its advantage of symmetry, the symmetric IPDG formulation requires a lot of computational effort to choose an optimal penalty parameter and compute different trace terms. To reduce such effort, we replace the derivatives of the velocity function with its weak derivatives computed by the geometric data of elements. Therefore, our modified EG (mEG) method is a penalty parameter-free numerical scheme that has reduced computational complexity and conserves the optimal convergence orders. Moreover, we achieve pressure robustness for the mEG method by employing a velocity reconstruction operator on the load vector on the right-hand side of the discrete system. The theoretical results are confirmed through numerical experiments with two- and three-dimensional examples.

1. Introduction

We consider the Stokes equations in a bounded domain $\Omega \subset \mathbb{R}^d$ for $d = 2, 3$ with simply connected Lipschitz boundary $\partial\Omega$: Find fluid velocity $\mathbf{u} : \Omega \to \mathbb{R}^d$ and pressure $p : \Omega \to \mathbb{R}$ such that

$$-\nu\Delta\mathbf{u} + \nabla p = \mathbf{f} \quad \text{in } \Omega, \tag{1.1a}$$

$$\nabla \cdot \mathbf{u} = 0 \quad \text{in } \Omega, \tag{1.1b}$$

$$\mathbf{u} = \mathbf{0} \quad \text{on } \partial\Omega, \tag{1.1c}$$

where $\nu > 0$ is a constant fluid viscosity, and $\mathbf{f}$ is a given body force.

In the finite element framework, finite-dimensional velocity and pressure spaces must satisfy the discrete inf-sup stability condition [1–3] to guarantee the well-posedness of the discrete problem corresponding to (1.1). Various mixed finite element methods (FEMs) have been developed under the discrete inf-sup condition, such as conforming and non-conforming mixed FEMs [4–6], discontinuous Galerkin methods [7,8], weak Galerkin methods [9,10], and enriched Galerkin methods [11,12]. These methods have been widely used for numerical simulations of the Stokes equations while providing different advantages.

For the Stokes equations, discontinuous Galerkin (DG) methods have received attention as advanced numerical methods with a locally conservative divergence-free condition and geometric flexibility on meshes. The interior penalty discontinuous Galerkin (IPDG) method is an example of DG methods, and it employs penalties to impose weakly the continuity of the solutions and boundary conditions. For example, the penalty formulation has also been adopted in enriched Galerkin methods for the Poisson equation [13,14] and C^0 interior penalty methods for the biharmonic equation [15]. It is well-known that a sufficiently large penalty parameter is required to ensure stability in the symmetric IPDG method. However, in numerical simulations, a large penalty parameter may increase the condition number of the stiffness matrix, leading to inaccurate simulation results. Also, the papers [16–18] discussed the mesh-dependent lower bounds for penalty parameters depending on the angles of mesh elements. Therefore, we pay special attention to constructing a penalty parameter-free scheme to resolve the difficulty in choosing proper penalty parameters. Various penalty parameter-free DG methods have been introduced for second-order elliptic problems by introducing extra degrees of freedom on edges/faces and auxiliary variables, e.g., hybrid high-order (HHO) methods [19], hybridizable discontinuous Galerkin (HDG) methods [20], and weak Galerkin (WG) methods [21]. By rewriting DG basis functions in the WG framework,

* Corresponding author.
E-mail addresses: seulip.lee@uga.edu (S. Lee), linmu@uga.edu (L. Mu).

https://doi.org/10.1016/j.camwa.2024.04.023
Received 6 July 2023; Received in revised form 4 April 2024; Accepted 19 April 2024
Available online 2 May 2024

another penalty parameter-free DG method [22], called a modified WG method, has been developed without increasing degrees of freedom. This idea inspires our work.

Our primary goal in this paper is to develop a low-cost and penalty parameter-free Stokes solver with optimal convergence orders. The enriched Galerkin (EG) velocity and pressure spaces have been presented in [12] for solving the Stokes equations with minimal degrees of freedom. The velocity space consists of linear Lagrange polynomials enriched by a discontinuous, piecewise linear, and mean-zero vector function per element, while piecewise constant functions approximate the pressure. A velocity function $\mathbf{v}$ can be expressed as $\mathbf{v} = \mathbf{v}^C + \mathbf{v}^D$, where $\mathbf{v}^C$ is a continuous linear Lagrange polynomial and $\mathbf{v}^D$ is a discontinuous piecewise linear enrichment function. Compared to the previous EG method [12] using the IPDG formulation, our modified EG (mEG) method is developed by replacing the derivatives of the velocity functions with their weak derivatives [23]. The weak derivatives are locally computed in each element by integration by parts using the interior function $\mathbf{v}$ and the average of $\mathbf{v}$ along edges/faces (we will provide details in Section 3). The weak derivatives for $\mathbf{v}^C$ remain the same as $\nabla\mathbf{v}^C$ and $\nabla\cdot\mathbf{v}^C$. For the discontinuous components $\mathbf{v}^D$, we compute the weak derivatives as piecewise constant functions by using the geometric data of each element, e.g., vertices, edges/faces, and area/volume. In the mEG method, the bilinear forms are simply assembled by the L^2-inner product of the weak derivatives and a parameter-free penalty term. The other trace terms in the IPDG formulation are not needed. Thus, the mEG method is penalty parameter-free, and its implementation is guaranteed to require reduced computational complexity. In the theoretical part, the coercivity and continuity of the bilinear form for the diffusion term in (1.1a) hold with no penalty parameter. Since the bilinear form for the divergence term (1.1b) remains the same as the original EG method, the discrete inf-sup condition of the mEG method can be inherited from the original one. Through two- and three-dimensional examples, we compare our modified EG method's and original EG methods' numerical performance with different penalty parameters. The numerical results demonstrate that our mEG method shows uniform stability and outperforms the original one.

Pressure robustness is an essential property of numerical methods for the Stokes equations in the case of small viscosity $\nu \ll 1$. In this case, inf-sup stable pairs may not guarantee accurate numerical velocity solutions. In standard mixed FEMs, including the EG method [12], the velocity error bounds are coupled with a pressure term inversely proportional to the viscosity ν. Thus, the numerical simulation for velocity may be destroyed by the factor $1/\nu$. In contrast, pressure-robust schemes can eliminate the pressure term from the velocity error bounds in the error estimates, so they guarantee accurate numerical velocity and pressure simultaneously. In some mixed FEMs, pressure robustness has been achieved by applying a velocity reconstruction operator [24] to the load vector on the right-hand side (see [25–31] as examples). More precisely, the exterior force $\mathbf{f} \in (L^2(\Omega))^d$ is decomposed as $\mathbf{f} = \boldsymbol{\eta} + \nabla\vartheta$ for some differentiable function ϑ and $\nabla\cdot\boldsymbol{\eta} = 0$. Then, it follows from integration by parts $(\nabla\vartheta, \bar{\mathbf{v}})_\Omega = (\vartheta, \nabla\cdot\bar{\mathbf{v}})_\Omega = 0$ for a divergence-free velocity $\bar{\mathbf{v}}$. Thus, a change of the exterior force $\mathbf{f} + \nabla\psi$ results in a solution $(\mathbf{u}, p+\psi)$. In a discretization with ϑ_h on a triangulation $\mathcal{T}_h$, we observe

$$(\nabla\vartheta_h, \bar{\mathbf{v}}_h)_\Omega = \sum_{T\in\mathcal{T}_h} \left[\langle\vartheta_h, \bar{\mathbf{v}}_h\cdot\mathbf{n}\rangle_{\partial T} - (\vartheta_h, \nabla\cdot\bar{\mathbf{v}}_h)_T\right] \neq 0,$$

where $\bar{\mathbf{v}}_h$ is a weakly divergence-free velocity, implying $(\vartheta_h, \nabla\cdot\bar{\mathbf{v}}_h)_T = 0$ for all $T \in \mathcal{T}_h$. However, the velocity reconstruction operator $\mathcal{R}$ mapping such velocity functions to an $H(\mathrm{div};\Omega)$-conforming finite element space leads to

$$\begin{aligned}(\nabla\vartheta_h, \mathcal{R}\bar{\mathbf{v}}_h)_\Omega &= \sum_{T\in\mathcal{T}_h} \left[\langle\vartheta_h, \mathcal{R}\bar{\mathbf{v}}_h\cdot\mathbf{n}\rangle_{\partial T} - (\vartheta_h, \nabla\cdot\mathcal{R}\bar{\mathbf{v}}_h)_T\right],\\ &= -\sum_{T\in\mathcal{T}_h} (\vartheta_h, \nabla\cdot\bar{\mathbf{v}}_h)_T = 0.\end{aligned}$$

To develop a pressure-robust scheme corresponding to the mEG method, we employ the velocity reconstruction operator [31], mapping the EG velocity test functions into the first-order Brezzi-Douglas-Marini space. Therefore, we achieve pressure robustness in the mEG method without compromising the optimal convergence orders.

The remaining sections of this paper are structured as follows: First, some important definitions, notations, and trace properties are introduced in Section 2. Section 3 recalls the EG method [12] and proposes the modified EG (mEG) method without a penalty parameter. In Section 4, we prove the well-posedness and error estimates of our mEG method. A pressure-robust mEG method is presented, and its robust error estimates are proved in Section 5. In Section 6, we validate our theoretical results through numerical experiments in two and three dimensions. We summarize our contribution in this paper and discuss related research in Section 7.

2. Preliminaries

To begin with, we introduce some notations and definitions used throughout this paper. For a bounded Lipschitz domain $D \in \mathbb{R}^d$, where $d = 2, 3$, we denote the Sobolev space as $H^s(D)$ for a real number $s \geq 0$. Its norm and seminorm are denoted by $\|\cdot\|_{s,D}$ and $|\cdot|_{s,D}$, respectively. The space $H^0(D)$ coincides with $L^2(D)$, and the L^2-inner product is denoted by $(\cdot,\cdot)_D$. When $D = \Omega$, the subscript D will be omitted. These notations are generalized to vector- and tensor-valued Sobolev spaces. The notation $H_0^1(D)$ means the space of $v \in H^1(D)$ such that $v = 0$ on ∂D, and $L_0^2(D)$ means the space of $v \in L^2(D)$ such that $(v,1)_D = 0$. The polynomial spaces of degree less than or equal to k are denoted as $P_k(D)$. We also introduce the Hilbert space

$$H(\mathrm{div}, D) := \{\mathbf{v} \in [L^2(D)]^d : \mathrm{div}\,\mathbf{v} \in L^2(D)\}$$

with the norm

$$\|\mathbf{v}\|^2_{H(\mathrm{div},D)} := \|\mathbf{v}\|^2_{0,D} + \|\mathrm{div}\,\mathbf{v}\|^2_{0,D}.$$

For discrete schemes, we assume that there exists a shape-regular triangulation $\mathcal{T}_h$ of Ω whose elements $T \in \mathcal{T}_h$ are triangles in two dimensions and tetrahedrons in three dimensions. Then, $\mathcal{E}_h$ denotes the collection of all edges/faces in $\mathcal{T}_h$, and $\mathcal{E}_h = \mathcal{E}_h^o \cup \mathcal{E}_h^b$, where $\mathcal{E}_h^o$ is the collection of all the interior edges/faces and $\mathcal{E}_h^b$ is that of the boundary edges/faces. For each element $T \in \mathcal{T}_h$, let h_T denote the diameter of T, and $\mathbf{n}_T$ (or $\mathbf{n}$) denote the outward unit normal vector on ∂T. For each interior edge/face $e \in \mathcal{E}_h^o$ shared by two adjacent elements T^+ and T^-, we let $\mathbf{n}_e$ be the unit normal vector from T^+ to T^-. For each $e \in \mathcal{E}_h^b$, $\mathbf{n}_e$ denotes the outward unit normal vector on $\partial\Omega$.

In a shape-regular triangulation $\mathcal{T}_h$, the broken Sobolev space is defined as

$$H^s(\mathcal{T}_h) = \{v \in L^2(\Omega) : v|_T \in H^s(T),\ \forall T \in \mathcal{T}_h\},$$

equipped with the norm

$$\|v\|_{s,\mathcal{T}_h} = \left(\sum_{T\in\mathcal{T}_h} \|v\|^2_{s,T}\right)^{1/2}.$$

When $s = 0$, the L^2-inner product on $\mathcal{T}_h$ is denoted by $(\cdot,\cdot)_{\mathcal{T}_h}$. Also, the L^2-inner product on $\mathcal{E}_h$ is denoted as $\langle\cdot,\cdot\rangle_{\mathcal{E}_h}$, and the L^2-norm on $\mathcal{E}_h$ is defined as

$$\|v\|_{0,\mathcal{E}_h} = \left(\sum_{e\in\mathcal{E}_h} \|v\|^2_{0,e}\right)^{1/2}.$$

The piecewise polynomial space corresponding to the broken Sobolev space is defined as

$$P_k(\mathcal{T}_h) = \{v \in L^2(\Omega) : v|_T \in P_k(T),\ \forall T \in \mathcal{T}_h\}.$$

In addition, the jump and average of v on $e \in \mathcal{E}_h$ are defined as

$$[v] = \begin{cases} v^+ - v^- & \text{on } e \in \mathcal{E}_h^o, \\ v & \text{on } e \in \mathcal{E}_h^b, \end{cases} \quad \{v\} = \begin{cases} (v^+ + v^-)/2 & \text{on } e \in \mathcal{E}_h^o, \\ v & \text{on } e \in \mathcal{E}_h^b, \end{cases}$$

where $v^{\pm}$ is the trace of $v|_{T^{\pm}}$ on $e \in \partial T^+ \cap \partial T^-$. These definitions are extended to vector- and tensor-valued functions.

We also introduce the trace properties mainly used in this paper. For any vector function $\mathbf{v}$ and scalar function q, we have

$$\sum_{T \in \mathcal{T}_h} \langle \mathbf{v} \cdot \mathbf{n}, q \rangle_{\partial T} = \langle [\mathbf{v}] \cdot \mathbf{n}_e, \{q\} \rangle_{\mathcal{E}_h} + \langle \{\mathbf{v}\} \cdot \mathbf{n}_e, [q] \rangle_{\mathcal{E}_h^o}. \tag{2.1}$$

For any function $v \in H^1(T)$, the following trace inequality holds

$$\|v\|_{0,e}^2 \le C \left(h_T^{-1} \|v\|_{0,T}^2 + h_T \|\nabla v\|_{0,T}^2 \right). \tag{2.2}$$

3. A modified enriched Galerkin method

We consider the weak formulation for the Stokes problem (1.1): Find $(\mathbf{u}, p) \in [H_0^1(\Omega)]^d \times L_0^2(\Omega)$ such that

$$\nu(\nabla \mathbf{u}, \nabla \mathbf{v}) - (\nabla \cdot \mathbf{v}, p) = (\mathbf{f}, \mathbf{v}), \quad \forall \mathbf{v} \in [H_0^1(\Omega)]^d, \tag{3.1a}$$

$$(\nabla \cdot \mathbf{u}, q) = 0, \qquad \forall q \in L_0^2(\Omega). \tag{3.1b}$$

In this manuscript, we focus on the homogeneous Dirichlet boundary condition for simplicity in analysis. The scheme can be extended to mixed boundary conditions, which will be briefly described in Section 6.

We recall the EG method [12] with its finite-dimensional velocity and pressure spaces and then introduce weak derivatives to establish the modified EG method in this section.

3.1. Standard enriched Galerkin method with interior penalty

We first introduce the EG finite dimensional velocity and pressure spaces. Let us denote the space of continuous components for velocity as

$$\mathbf{C}_h = \{\mathbf{v}^C \in [H_0^1(\Omega)]^d : \mathbf{v}^C|_T \in [P_1(T)]^d, \ \forall T \in \mathcal{T}_h\}.$$

The space of discontinuous components for velocity is defined as

$$\mathbf{D}_h = \{\mathbf{v}^D \in L^2(\Omega) : \mathbf{v}^D|_T = c(\mathbf{x} - \mathbf{x}_T), \ c \in \mathbb{R}, \ \forall T \in \mathcal{T}_h\},$$

where $\mathbf{x}_T$ is the barycenter of $T \in \mathcal{T}_h$. Then, the EG finite dimensional velocity space is defined as

$$\mathbf{V}_h = \mathbf{C}_h \oplus \mathbf{D}_h,$$

that is, any function $\mathbf{v} \in \mathbf{V}_h$ consists of unique continuous and discontinuous components, $\mathbf{v} = \mathbf{v}^C + \mathbf{v}^D$ for $\mathbf{v}^C \in \mathbf{C}_h$ and $\mathbf{v}^D \in \mathbf{D}_h$. At the same time, the EG pressure space is chosen as

$$Q_h = \{q \in L_0^2(\Omega) : q|_T \in P_0(T), \ \forall T \in \mathcal{T}_h\}.$$

Therefore, the EG method [12] is formulated with the pair of the spaces $\mathbf{V}_h \times Q_h$.

Algorithm 1 Enriched Galerkin (EG) method.

Find $(\mathbf{u}_h, p_h) \in \mathbf{V}_h \times Q_h$ such that

$$\mathbf{a}(\mathbf{u}_h, \mathbf{v}) - \mathbf{b}(\mathbf{v}, p_h) = (\mathbf{f}, \mathbf{v}), \quad \forall \mathbf{v} \in \mathbf{V}_h, \tag{3.2a}$$

$$\mathbf{b}(\mathbf{u}_h, q) = 0, \qquad \forall q \in Q_h, \tag{3.2b}$$

where

$$\mathbf{a}(\mathbf{w}, \mathbf{v}) := \nu \big((\nabla \mathbf{w}, \nabla \mathbf{v})_{\mathcal{T}_h} - \langle \{\nabla \mathbf{w}\} \cdot \mathbf{n}_e, [\mathbf{v}] \rangle_{\mathcal{E}_h} - \langle \{\nabla \mathbf{v}\} \cdot \mathbf{n}_e, [\mathbf{w}] \rangle_{\mathcal{E}_h} + \rho \langle h_e^{-1} [\mathbf{w}], [\mathbf{v}] \rangle_{\mathcal{E}_h} \big), \tag{3.3a}$$

$$\mathbf{b}(\mathbf{w}, q) := (\nabla \cdot \mathbf{w}, q)_{\mathcal{T}_h} - \langle [\mathbf{w}] \cdot \mathbf{n}_e, \{q\} \rangle_{\mathcal{E}_h}. \tag{3.3b}$$

Here, $\rho > 0$ is a penalty parameter and $h_e = |e|^{1/(d-1)}$, where $|e|$ is the length/area of the edge/face $e \in \mathcal{E}_h$.

In Algorithm 1, the symmetric interior penalty discontinuous Galerkin (IPDG) formulation is adopted to weakly impose the continuity of the discontinuous component $\mathbf{v}^D \in \mathbf{D}_h$, and it requires a sufficiently large penalty parameter ρ to guarantee the well-posedness of the method (see [12] for details). Other non-symmetric formulations have also been discussed in [12].

3.2. Modified enriched Galerkin method with weak derivatives

We introduce a weak Galerkin (WG) finite element space for velocity [9],

$$\mathcal{V}_h = \{\upsilon = \{\upsilon_0, \upsilon_b\} \mid \upsilon_0|_T \in [P_1(T)]^d, \ \forall T \in \mathcal{T}_h, \ \upsilon_b|_e \in [P_1(e)]^d, \ \forall e \in \mathcal{E}_h\}.$$

Then, the EG velocity $\mathbf{v} \in \mathbf{V}_h$ can be viewed as a WG function in $\mathcal{V}_h$, that is,

$$\upsilon_0 = \mathbf{v}, \quad \upsilon_b = \{\mathbf{v}\} \quad \Rightarrow \quad \{\mathbf{v}, \{\mathbf{v}\}\} \in \mathcal{V}_h,$$

and the weak derivatives for $\mathbf{v} \in \mathbf{V}_h$ are locally defined as follows.

Definition 3.1. The weak gradient operator [23] is defined as $\nabla_w \upsilon|_T \in [P_0(T)]^{d \times d}$ when $\upsilon = \{\upsilon_0, \upsilon_b\} \in \mathcal{V}_h$ satisfying

$$(\nabla_w \upsilon, \aleph)_T = \langle \upsilon_b, \aleph \cdot \mathbf{n} \rangle_{\partial T}, \quad \forall \aleph \in [P_0(T)]^{d \times d}.$$

In a similar manner, the weak gradient for the EG velocity $\mathbf{v} \in \mathbf{V}_h$ is defined as $\nabla_w \mathbf{v}|_T \in [P_0(T)]^{d \times d}$ such that

$$(\nabla_w \mathbf{v}, \aleph)_T = \langle \{\mathbf{v}\}, \aleph \cdot \mathbf{n} \rangle_{\partial T}, \quad \forall \aleph \in [P_0(T)]^{d \times d}.$$

Moreover, the weak divergence operator [23] for $\mathbf{v} \in \mathbf{V}_h$ is defined as $\nabla_w \cdot \mathbf{v}|_T \in P_0(T)$ such that

$$(\nabla_w \cdot \mathbf{v}, q)_T = \langle \{\mathbf{v}\} \cdot \mathbf{n}, q \rangle_{\partial T}, \quad \forall q \in P_0(T).$$

The weak gradient $\nabla_w \mathbf{v} \in [P_0(T)]^{d \times d}$ is equivalent to the discrete gradient $G_h^0(\mathbf{v}) \in [P_0(T)]^{d \times d}$ introduced in the discontinuous Galerkin literature [32, Section 4.3]. Moreover, such equivalence holds for any polynomial degree k. The WG method uses a different bilinear form from the symmetric IPDG bilinear form.

Remark 3.2. For any EG velocity function $\mathbf{v} \in \mathbf{V}_h$, the differences between the weak derivatives and regular derivatives are given as

$$\big(\nabla \mathbf{v} - \nabla_w \mathbf{v}, \aleph\big)_{\mathcal{T}_h} = \langle [\mathbf{v}], \{\aleph\} \cdot \mathbf{n}_e \rangle_{\mathcal{E}_h}, \quad \forall \aleph \in [P_0(\mathcal{T}_h)]^{d \times d}, \tag{3.4a}$$

$$\big(\nabla \cdot \mathbf{v} - \nabla_w \cdot \mathbf{v}, q\big)_{\mathcal{T}_h} = \langle [\mathbf{v}] \cdot \mathbf{n}_e, \{q\} \rangle_{\mathcal{E}_h}, \quad \forall q \in P_0(\mathcal{T}_h). \tag{3.4b}$$

These identities are simply obtained from the definition of the weak derivatives and integration by parts. Since the EG velocity consists of $\mathbf{v}^C \in \mathbf{C}_h$ and $\mathbf{v}^D \in \mathbf{D}_h$, it is clear to see from (3.4) that $\nabla_w \mathbf{v}^C = \nabla \mathbf{v}^C$, $\nabla_w \cdot \mathbf{v}^C = \nabla \cdot \mathbf{v}^C$, and the jumps of $\mathbf{v}^D$ on $e \in \mathcal{E}_h^o$ cause the differences. In practice, the weak gradient $\nabla_w \mathbf{v}^D$ is locally determined by

$$(\nabla_w \mathbf{v}^D)_{i,j} = \frac{n_j}{|T|}\langle \{\mathbf{v}^D\}, \mathbf{e}_i\rangle_{\partial T}, \quad 1 \le i,j \le d,$$

where n_j is the j-th component of $\mathbf{n}$ and $\mathbf{e}_i$ is the standard unit vector whose i-th component is 1. Since $\mathbf{v}^D|_T = c(\mathbf{x} - \mathbf{x}_T)$ is a linear function, the above line/surface integral can be simply computed by the one-point quadrature rule on each edge/face, respectively. Also, the weak divergence $\nabla_w \cdot \mathbf{v}^D$ is the trace of $\nabla_w \mathbf{v}^D$ from the definition, which implies no associated cost in computing the weak divergence.

Therefore, we propose the modified enriched Galerkin method which is formulated by the weak derivatives for the EG velocity $\mathbf{v} \in \mathbf{V}_h$.

Algorithm 2 Modified enriched Galerkin (mEG) method.

Find $(\mathbf{u}_h, p_h) \in \mathbf{V}_h \times Q_h$ such that

$$\mathbf{a}_w(\mathbf{u}_h, \mathbf{v}) - \mathbf{b}_w(\mathbf{v}, p_h) = (\mathbf{f}, \mathbf{v}), \quad \forall \mathbf{v} \in \mathbf{V}_h, \tag{3.5a}$$

$$\mathbf{b}_w(\mathbf{u}_h, q) = 0, \quad \forall q \in Q_h, \tag{3.5b}$$

where

$$\mathbf{a}_w(\mathbf{w}, \mathbf{v}) := \nu\big((\nabla_w \mathbf{w}, \nabla_w \mathbf{v})_{\mathcal{T}_h} + \langle h_e^{-1}[\mathbf{w}], [\mathbf{v}]\rangle_{\mathcal{E}_h}\big), \tag{3.6a}$$

$$\mathbf{b}_w(\mathbf{w}, q) := (\nabla_w \cdot \mathbf{w}, q)_{\mathcal{T}_h}. \tag{3.6b}$$

In this case, $h_e = |e|^{1/(d-1)}$, where $|e|$ is the length/area of the edge/face $e \in \mathcal{E}_h$.

Remark 3.3. There is no penalty parameter in the mEG method, while the EG method in Algorithm 1 requires a sufficiently large penalty parameter ρ. Inspired by [23,33], the bilinear form $\mathbf{a}_w(\cdot,\cdot)$ has a penalty term but does not contain a penalty parameter to tune. More precisely, $\mathbf{a}_w(\mathbf{v},\mathbf{v})$ directly defines a mesh-dependent norm, which naturally implies the bilinear form's coercivity without a penalty parameter. We will show details in Section 4.

In addition, the identity (3.4b) implies that for any $\mathbf{w} \in \mathbf{V}_h$ and $q \in Q_h$,

$$\mathbf{b}_w(\mathbf{w}, q) = \mathbf{b}(\mathbf{w}, q), \tag{3.7}$$

which makes it simple to prove the discrete inf-sup condition. In practice, this allows us to use the same block matrices corresponding to $\mathbf{b}(\cdot,\cdot)$ (or $\mathbf{b}_w(\cdot,\cdot)$) for both EG and mEG methods.

4. Well-posedness and error analysis

For the EG method [12] in Algorithm 1, the well-posedness and error estimates have been proved in terms of the energy norm in $\mathbf{V}_h$,

$$\|\mathbf{v}\|_{\mathcal{E}} := \Big(\|\nabla \mathbf{v}\|_{0,\mathcal{T}_h}^2 + \rho\|h_e^{-1/2}[\mathbf{v}]\|_{0,\mathcal{E}_h}^2\Big)^{\frac{1}{2}}.$$

To show the discrete inf-sup condition and a priori error estimates for the mEG method in Algorithm 2, we employ the theoretical results of the EG method. In this case, the mEG method includes the weak derivatives, so it requires a mesh-dependent norm corresponding to the bilinear form $\mathbf{a}_w(\cdot,\cdot)$,

$$|||\mathbf{v}||| := \Big(\|\nabla_w \mathbf{v}\|_{0,\mathcal{T}_h}^2 + \|h_e^{-1/2}[\mathbf{v}]\|_{0,\mathcal{E}_h}^2\Big)^{\frac{1}{2}}.$$

Then, the following norm equivalence helps to prove the theoretical results of the mEG method.

Lemma 4.1. *For any $\mathbf{v} \in \mathbf{V}_h$, there are positive constants γ_* and γ^* independent of $h := \max_{T\in\mathcal{T}_h} h_T$ such that*

$$\gamma_* |||\mathbf{v}||| \le \|\mathbf{v}\|_{\mathcal{E}} \le \gamma^* |||\mathbf{v}|||. \tag{4.1}$$

Proof. We start with the relation (3.4a) while choosing $\aleph = \nabla_w \mathbf{v}$,

$$\|\nabla_w \mathbf{v}\|_{0,\mathcal{T}_h}^2 = \big(\nabla_w \mathbf{v}, \nabla_w \mathbf{v}\big)_{\mathcal{T}_h} = \big(\nabla \mathbf{v}, \nabla_w \mathbf{v}\big)_{\mathcal{T}_h} - \langle [\mathbf{v}], \{\nabla_w \mathbf{v}\} \cdot \mathbf{n}_e\rangle_{\mathcal{E}_h^o}.$$

Then, the first term is simply bounded using the Cauchy-Schwarz inequality,

$$\big(\nabla \mathbf{v}, \nabla_w \mathbf{v}\big)_{\mathcal{T}_h} \le \|\nabla \mathbf{v}\|_{0,\mathcal{T}_h} \|\nabla_w \mathbf{v}\|_{0,\mathcal{T}_h},$$

and the second term is bounded using the Cauchy-Schwarz inequality and trace inequality (2.2),

$$\begin{aligned}\langle [\mathbf{v}], \{\nabla_w \mathbf{v}\} \cdot \mathbf{n}_e\rangle_{\mathcal{E}_h^o} &\le \|h_e^{-1/2}[\mathbf{v}]\|_{0,\mathcal{E}_h^o} \|h_e^{1/2}\{\nabla_w \mathbf{v}\}\|_{0,\mathcal{E}_h^o} \\ &\le C\|h_e^{-1/2}[\mathbf{v}]\|_{0,\mathcal{E}_h^o} \|\nabla_w \mathbf{v}\|_{0,\mathcal{T}_h}.\end{aligned}$$

Hence, we arrive at

$$\|\nabla_w \mathbf{v}\|_{0,\mathcal{T}_h} \le C\|\mathbf{v}\|_{\mathcal{E}},$$

which implies the lower bound in (4.1).

On the other hand, we choose $\aleph = \nabla \mathbf{v}$ in (3.4a) and apply the Cauchy-Schwarz inequality and (2.2) to obtain

$$\|\nabla \mathbf{v}\|_{0,\mathcal{T}_h}^2 \le \big(\nabla_w \mathbf{v}, \nabla \mathbf{v}\big)_{\mathcal{T}_h} + \langle [\mathbf{v}], \{\nabla \mathbf{v}\} \cdot \mathbf{n}_e\rangle_{\mathcal{E}_h^o} \le C|||\mathbf{v}|||\|\nabla \mathbf{v}\|_{0,\mathcal{T}_h}.$$

Therefore, it is clear to see that

$$\|\nabla \mathbf{v}\|_{0,\mathcal{T}_h} \le C|||\mathbf{v}|||,$$

which yields the upper bound in (4.1). □

4.1. Well-posedness

In this subsection, with the norm equivalence (4.1), we show the well-posedness of the mEG method by proving the essential properties of the bilinear forms. Let $\Pi_h : [H^2(\Omega)]^d \to \mathbf{V}_h$ be the interpolation operator [34] such that

$$\Pi_h \mathbf{v} = \Pi_h^C \mathbf{v} + \Pi_h^D \mathbf{v},$$

where $\Pi_h^C \mathbf{v} \in \mathbf{C}_h$ is the nodal value interpolant of $\mathbf{v}$ and $\Pi_h^D \mathbf{v} \in \mathbf{D}_h$ satisfies $(\nabla \cdot \Pi_h^D \mathbf{v}, 1)_T = (\nabla \cdot (\mathbf{v} - \Pi_h^C \mathbf{v}), 1)_T$ for all $T \in \mathcal{T}_h$. The corresponding interpolation error estimates [34] are as follows:

$$|\mathbf{v} - \Pi_h \mathbf{v}|_{j,\mathcal{T}_h} \le Ch^{m-j}|\mathbf{v}|_m, \quad 0 \le j \le m \le 2, \quad \forall \mathbf{v} \in [H^2(\Omega)]^d, \tag{4.2a}$$

$$\|\mathbf{v} - \Pi_h \mathbf{v}\|_{\mathcal{E}} \le Ch\|\mathbf{v}\|_2, \quad \forall \mathbf{v} \in [H^2(\Omega)]^d. \tag{4.2b}$$

Lemma 4.2. *There exists a positive constant C independent of h and ν such that*

$$\inf_{q\in Q_h} \sup_{\mathbf{v}\in\mathbf{V}_h} \frac{\mathbf{b}_w(\mathbf{v}, q)}{|||\mathbf{v}|||\|q\|_0} \ge C. \tag{4.3}$$

Proof. We first cite the results of discrete inf-sup condition in [12]. For any $q \in Q_h \subset L_0^2(\Omega)$, there exist a vector $\mathbf{v} \in [H_0^1(\Omega)]^d$ and a constant $C_{\mathcal{E}} > 0$ independent of h and ν such that

$$\frac{\mathbf{b}(\Pi_h \mathbf{v}, q)}{\|\Pi_h \mathbf{v}\|_{\mathcal{E}}} \ge C_{\mathcal{E}}\|q\|_0.$$

Hence, it follows from (3.7) and (4.1) that

$$\frac{\mathbf{b}_w(\Pi_h \mathbf{v}, q)}{|||\Pi_h \mathbf{v}|||} \ge \gamma_* C_{\mathcal{E}}\|q\|_0. \quad \square$$

It is also straightforward to show the continuity of $\mathbf{b}_w(\cdot,\cdot)$ with respect to the norm $|||\cdot|||$ using the norm equivalence (4.1).

Lemma 4.3. *For any $\mathbf{v} \in \mathbf{V}_h$ and $q \in Q_h$, there exists a positive constant C independent of h satisfying*

$$|\mathbf{b}_w(\mathbf{v},q)| \le C\|q\|_0|||\mathbf{v}|||. \tag{4.4}$$

Proof. It follows from (3.7), (4.1), and the continuity of $\mathbf{b}(\cdot,\cdot)$ in [12] that

$$|\mathbf{b}_w(\mathbf{v},q)| = |\mathbf{b}(\mathbf{v},q)| \le C\|q\|_0\|\mathbf{v}\|_{\mathcal{E}} \le C\gamma^*\|q\|_0|||\mathbf{v}|||. \quad \square$$

In addition, we obtain the coercivity and continuity of $\mathbf{a}_w(\cdot,\cdot)$ with respect to $|||\cdot|||$. (See [23] for details.)

Lemma 4.4. *For any $\mathbf{v},\mathbf{w} \in \mathbf{V}_h$, we have the coercivity and continuity results for $\mathbf{a}_w(\cdot,\cdot)$:*

$$\mathbf{a}_w(\mathbf{v},\mathbf{v}) = \nu|||\mathbf{v}|||^2, \tag{4.5}$$

$$|\mathbf{a}_w(\mathbf{v},\mathbf{w})| \le \nu|||\mathbf{v}|||||\mathbf{w}|||. \tag{4.6}$$

Thus, we obtain the well-posedness of the mEG method.

Theorem 4.5. *There exists a unique solution $(\mathbf{u}_h,p_h) \in \mathbf{V}_h \times Q_h$ to the mEG method in Algorithm 2.*

Proof. Since $\mathbf{V}_h$ and Q_h are finite dimensional spaces, it suffices to show that $\mathbf{u}_h = \mathbf{0}$ and $p_h = 0$ when $\mathbf{f} = \mathbf{0}$. If we choose $\mathbf{v} = \mathbf{u}_h$ in (3.5a) and $q = p_h$ in (3.5b) and add the two equations, then we obtain

$$\mathbf{a}_w(\mathbf{u}_h,\mathbf{u}_h) = 0.$$

Thus, it follows from (4.5) that $|||\mathbf{u}_h||| = 0$, so $\mathbf{u}_h = \mathbf{0}$. Moreover, the fact $\mathbf{u}_h = \mathbf{0}$ in (3.5) implies

$$\mathbf{b}_w(\mathbf{v},p_h) = 0, \quad \forall \mathbf{v} \in \mathbf{V}_h.$$

Therefore, we have $\|p_h\|_0 = 0$ from (4.3), which gives $p_h = 0$. $\square$

4.2. Error estimates

We prove error estimates for velocity and pressure with respect to the mesh-dependent norm $|||\cdot|||$ and the L^2-norm, respectively. We first introduce the local L^2-projection $\mathcal{P}_0 : H^1(\Omega) \to Q_h$ satisfying $(q - \mathcal{P}_0 q, 1)_T = 0$ for all $T \in \mathcal{T}_h$ and its error estimate,

$$\|q - \mathcal{P}_0 q\|_0 \le Ch\|q\|_1, \quad \forall q \in H^1(\Omega). \tag{4.7}$$

Furthermore, let us define $\Theta_h : [H^2(\Omega)]^d \to \mathcal{V}_h$ as

$$\Theta_h\mathbf{u} = \{\Theta_0\mathbf{u}, \Theta_b\mathbf{u}\},$$

where Θ_0 and Θ_b are the local L^2-projections onto $[P_1(T)]^d$ for all $T \in \mathcal{T}_h$ and $[P_1(e)]^d$ for all $e \in \mathcal{E}_h$, respectively. Then, we have the following commutative property [9],

$$\nabla_w(\Theta_h\mathbf{v}) = \mathbf{\Theta}_h(\nabla\mathbf{v}), \tag{4.8}$$

where $\mathbf{\Theta}_h$ is the local L^2-projection onto $[P_0(T)]^{d\times d}$.

We define error functions used in the error estimates,

$$\chi_h = \mathbf{u} - \Pi_h\mathbf{u}, \quad \mathbf{e}_h = \Pi_h\mathbf{u} - \mathbf{u}_h, \quad \xi_h = p - \mathcal{P}_0 p, \quad \epsilon_h = \mathcal{P}_0 p - p_h. \tag{4.9}$$

Then, we derive the main error equations in the following lemma.

Lemma 4.6. *For any $\mathbf{v} \in \mathbf{V}_h$ and $q \in Q_h$, we have*

$$\mathbf{a}_w(\mathbf{e}_h,\mathbf{v}) - \mathbf{b}_w(\mathbf{v},\epsilon_h) = l_1(\mathbf{u},\mathbf{v}) + l_2(\mathbf{u},\mathbf{v}) + \mathbf{s}(\Pi_h\mathbf{u},\mathbf{v}) + \mathbf{b}_w(\mathbf{v},\xi_h), \tag{4.10a}$$

$$\mathbf{b}_w(\mathbf{e}_h,q) = -\mathbf{b}_w(\chi_h,q), \tag{4.10b}$$

where the supplemental bilinear forms are defined as follows:

$$l_1(\mathbf{u},\mathbf{v}) = \nu\sum_{T\in\mathcal{T}_h}\langle\nabla\mathbf{u}\cdot\mathbf{n} - \mathbf{\Theta}_h(\nabla\mathbf{u})\cdot\mathbf{n}, \mathbf{v} - \{\mathbf{v}\}\rangle_{\partial T},$$

$$l_2(\mathbf{u},\mathbf{v}) = \nu\left(\nabla_w(\Pi_h\mathbf{u} - \Theta_h\mathbf{u}), \nabla_w\mathbf{v}\right)_{\mathcal{T}_h},$$

$$\mathbf{s}(\Pi_h\mathbf{u},\mathbf{v}) = \nu\langle h_e^{-1}[\Pi_h\mathbf{u}],[\mathbf{v}]\rangle_{\mathcal{E}_h}.$$

Proof. For any $\mathbf{v} \in \mathbf{V}_h$, integration by parts and the definition of $\mathbf{\Theta}_h$ imply

$$\begin{aligned}(-\Delta\mathbf{u},\mathbf{v})_{\mathcal{T}_h} &= -\sum_{T\in\mathcal{T}_h}\langle\nabla\mathbf{u}\cdot\mathbf{n},\mathbf{v}\rangle_{\partial T} + (\nabla\mathbf{u},\nabla\mathbf{v})_{\mathcal{T}_h}\\ &= -\sum_{T\in\mathcal{T}_h}\langle\nabla\mathbf{u}\cdot\mathbf{n},\mathbf{v}-\{\mathbf{v}\}\rangle_{\partial T} + \left(\mathbf{\Theta}_h(\nabla\mathbf{u}),\nabla\mathbf{v}\right)_{\mathcal{T}_h}.\end{aligned}$$

Then, the definition of the weak gradient and the commutative property (4.8) lead to

$$\begin{aligned}\left(\mathbf{\Theta}_h(\nabla\mathbf{u}),\nabla\mathbf{v}\right)_{\mathcal{T}_h} &= \left(\mathbf{\Theta}_h(\nabla\mathbf{u}),\nabla_w\mathbf{v}\right)_{\mathcal{T}_h} + \left(\mathbf{\Theta}_h(\nabla\mathbf{u}),\nabla\mathbf{v}-\nabla_w\mathbf{v}\right)_{\mathcal{T}_h}\\ &= \left(\nabla_w(\Theta_h\mathbf{u}),\nabla_w\mathbf{v}\right)_{\mathcal{T}_h} + \sum_{T\in\mathcal{T}_h}\langle\mathbf{\Theta}_h(\nabla\mathbf{u})\cdot\mathbf{n},\mathbf{v}-\{\mathbf{v}\}\rangle_{\partial T}.\end{aligned}$$

Hence, we obtain

$$(-\Delta\mathbf{u},\mathbf{v})_{\mathcal{T}_h} = \left(\nabla_w(\Theta_h\mathbf{u}),\nabla_w\mathbf{v}\right)_{\mathcal{T}_h} - \sum_{T\in\mathcal{T}_h}\langle\nabla\mathbf{u}\cdot\mathbf{n} - \mathbf{\Theta}_h(\nabla\mathbf{u})\cdot\mathbf{n},\mathbf{v}-\{\mathbf{v}\}\rangle_{\partial T},$$

$$(\nabla p,\mathbf{v})_{\mathcal{T}_h} = \mathbf{b}_w(\mathbf{v},p),$$

where the second equation is obtained by the trace identity (2.1), the continuity of p, and (3.4b). Then, by combining the above two equations in the equation (1.1a), we have

$$\left(\nabla_w(\Theta_h\mathbf{u}),\nabla_w\mathbf{v}\right)_{\mathcal{T}_h} - \mathbf{b}_w(\mathbf{v},p) = (\mathbf{f},\mathbf{v}) + l_1(\mathbf{u},\mathbf{v}).$$

If we add proper terms including $\Pi_h\mathbf{u}$ to both sides and subtract $\mathbf{b}_w(\mathbf{v},P_0p)$ from both sides, we get

$$\mathbf{a}_w(\Pi_h\mathbf{u},\mathbf{v}) - \mathbf{b}_w(\mathbf{v},\mathcal{P}_0p) = (\mathbf{f},\mathbf{v}) + l_1(\mathbf{u},\mathbf{v}) + l_2(\mathbf{u},\mathbf{v}) + \mathbf{s}(\Pi_h\mathbf{u},\mathbf{v}) + \mathbf{b}_w(\mathbf{v},\xi_h).$$

By comparing this equation with (3.5a) in the mEG method, we arrive at

$$\mathbf{a}_w(\mathbf{e}_h,\mathbf{v}) - \mathbf{b}_w(\mathbf{v},\epsilon_h) = l_1(\mathbf{u},\mathbf{v}) + l_2(\mathbf{u},\mathbf{v}) + \mathbf{s}(\Pi_h\mathbf{u},\mathbf{v}) + \mathbf{b}_w(\mathbf{v},\xi_h).$$

Furthermore, the continuity of $\mathbf{u}$ and (3.5b) imply

$$(\nabla\cdot\mathbf{u},q)_{\mathcal{T}_h} = \mathbf{b}_w(\mathbf{u},q) = 0 = \mathbf{b}_w(\mathbf{u}_h,q),$$

so (4.10b) is obtained by subtracting $\mathbf{b}_w(\Pi_h\mathbf{u},q)$ from both sides. $\square$

We provide the upper bounds for the supplementary bilinear forms in Lemma 4.6.

Lemma 4.7. *We assume that $\mathbf{w} \in [H^2(\Omega)]^d$ and $\mathbf{v} \in \mathbf{V}_h$. Then, we have*

$$|l_1(\mathbf{w},\mathbf{v})| \le C\nu h\|\mathbf{w}\|_2|||\mathbf{v}|||, \tag{4.11a}$$

$$|l_2(\mathbf{w},\mathbf{v})| \le C\nu h\|\mathbf{w}\|_2|||\mathbf{v}|||, \tag{4.11b}$$

$$|\mathbf{s}(\Pi_h\mathbf{w},\mathbf{v})| \le C\nu h\|\mathbf{w}\|_2|||\mathbf{v}|||, \tag{4.11c}$$

where the constant C is independent of h.

Proof. The proof of the bound (4.11a) can be found in [23], so we focus on showing (4.11b) and (4.11c) here. The definition of the weak gradient and the properties of the projections Π_h and Θ_h lead to

$$\begin{aligned}|l_2(\mathbf{w},\mathbf{v})| &= \nu\left|\left(\nabla_w(\Pi_h\mathbf{w} - \Theta_h\mathbf{w}),\nabla_w\mathbf{v})\right)_{\mathcal{T}_h}\right|\\ &= \nu\left|\sum_{T\in\mathcal{T}_h}\langle\{\Pi_h\mathbf{w}\} - \Theta_b\mathbf{w},\nabla_w\mathbf{v}\cdot\mathbf{n}\rangle_{\partial T}\right|\end{aligned}$$

$$
\begin{aligned}
&= \nu \left| \sum_{T\in\mathcal{T}_h} \langle \{\Pi_h \mathbf{w} - \mathbf{w}\}, \nabla_w \mathbf{v}\cdot\mathbf{n}\rangle_{\partial T} \right| \\
&\le \nu \sum_{T\in\mathcal{T}_h} \|h_T^{-1/2}\{\Pi_h\mathbf{w}-\mathbf{w}\}\|_{\partial T} \|h_T^{1/2}\nabla_w\mathbf{v}\|_{\partial T} \\
&\le C\nu h \|\mathbf{w}\|_2 \|\nabla_w \mathbf{v}\|_{0,\mathcal{T}_h}
\end{aligned}
$$

The third identity holds true because $\mathbf{w}\in[H^2(\Omega)]^d$ is continuous on ∂T, and the last inequality is obtained from the trace inequality (2.2) and (4.2a).

For the stabilization term (4.11c), it follows from the Cauchy-Schwarz inequality, (2.2), and (4.2a) that

$$
\begin{aligned}
|\mathbf{s}(\Pi_h\mathbf{w},\mathbf{v})| &= \nu \left| \langle h_e^{-1}[\Pi_h\mathbf{w}-\mathbf{w}], [\mathbf{v}]\rangle_{\mathcal{E}_h} \right| \\
&\le C\nu \|h_e^{-1/2}[\Pi_h\mathbf{w}-\mathbf{w}]\|_{0,\mathcal{E}_h} \|h_e^{-1/2}[\mathbf{v}]\|_{0,\mathcal{E}_h} \\
&\le C\nu h \|\mathbf{w}\|_2 |||\mathbf{v}|||. \quad \square
\end{aligned}
$$

Consequently, we obtain the following error estimates.

Theorem 4.8. *Let $(\mathbf{u},p)\in[H_0^1(\Omega)\cap H^2(\Omega)]^d\times(L_0^2(\Omega)\cap H^1(\Omega))$ be the solution to (1.1a)-(1.1c), and $(\mathbf{u}_h,p_h)\in\mathbf{V}_h\times Q_h$ be the discrete solution from the* mEG *method. Then, we have the following error estimates*

$$
\begin{aligned}
&|||\Pi_h\mathbf{u}-\mathbf{u}_h||| \le Ch\left(\|\mathbf{u}\|_2 + \frac{1}{\nu}\|p\|_1\right), \\
&\|\mathcal{P}_0 p - p_h\|_0 \le Ch\left(\nu\|\mathbf{u}\|_2 + \|p\|_1\right).
\end{aligned}
$$

Proof. First, we see the error equation (4.10a), for any $\mathbf{v}\in\mathbf{V}_h$ and $q\in Q_h$,

$$
\mathbf{b}_w(\mathbf{v},\epsilon_h) = \mathbf{a}_w(\mathbf{e}_h,\mathbf{v}) - l_1(\mathbf{u},\mathbf{v}) - l_2(\mathbf{u},\mathbf{v}) - \mathbf{s}(\Pi_h\mathbf{u},\mathbf{v}) - \mathbf{b}_w(\mathbf{v},\xi_h).
$$

Then, it follows from (4.6), (4.11), (4.4), and (4.7) that

$$
\begin{aligned}
|\mathbf{b}_w(\mathbf{v},\epsilon_h)| &\le C\left(\nu|||\mathbf{e}_h|||\,|||\mathbf{v}||| + \nu h\|\mathbf{u}\|_2|||\mathbf{v}||| + \|\xi_h\|_0|||\mathbf{v}|||\right) \\
&\le C\left(\nu|||\mathbf{e}_h||| + \nu h\|\mathbf{u}\|_2 + h\|p\|_1\right)|||\mathbf{v}|||.
\end{aligned}
$$

The inf-sup condition (4.3) implies that

$$
\|\epsilon_h\|_0 \le C\left(\nu|||\mathbf{e}_h||| + h(\nu\|\mathbf{u}\|_2 + \|p\|_1)\right). \tag{4.12}
$$

Moreover, by choosing $\mathbf{v}=\mathbf{e}_h$ and $q=\epsilon_h$ in (4.10) and substituting (4.10b) into (4.10a), we obtain

$$
\mathbf{a}_w(\mathbf{e}_h,\mathbf{e}_h) = -\mathbf{b}_w(\chi_h,\epsilon_h) + l_1(\mathbf{u},\mathbf{e}_h) + l_2(\mathbf{u},\mathbf{e}_h) + \mathbf{s}(\Pi_h\mathbf{u},\mathbf{e}_h) + \mathbf{b}_w(\mathbf{e}_h,\xi_h).
$$

Here, we show an upper bound for the term $\mathbf{b}_w(\chi_h,\epsilon_h)$. Integration by parts and the trace identity (2.1) give

$$
\begin{aligned}
\mathbf{b}_w(\chi_h,\epsilon_h) &= \mathbf{b}(\chi_h,\epsilon_h) \\
&= \left(\nabla\cdot\chi_h,\epsilon_h\right)_{\mathcal{T}_h} - \langle[\chi_h]\cdot\mathbf{n}_e,\{\epsilon_h\}\rangle_{\mathcal{E}_h} \\
&= \sum_{T\in\mathcal{T}_h}\langle\chi_h\cdot\mathbf{n},\epsilon_h\rangle_{\partial T} - \langle[\chi_h]\cdot\mathbf{n}_e,\{\epsilon_h\}\rangle_{\mathcal{E}_h} \\
&= \langle\{\chi_h\}\cdot\mathbf{n}_e,[\epsilon_h]\rangle_{\mathcal{E}_h^o}.
\end{aligned}
$$

Thus, it follows from the Cauchy-Schwarz inequality, (2.2), and (4.2a) that

$$
|\mathbf{b}_w(\chi_h,\epsilon_h)| \le \|\{\chi_h\}\|_{0,\mathcal{E}_h}\|[\epsilon_h]\|_{0,\mathcal{E}_h} \le Ch\|\mathbf{u}\|_2\|\epsilon_h\|_0. \tag{4.13}
$$

Hence, by (4.5), (4.11), (4.4), (4.7), (4.12), and (4.13), we have

$$
\nu|||\mathbf{e}_h|||^2 \le C\left(\nu h\|\mathbf{u}\|_2|||\mathbf{e}_h||| + h\|p\|_1|||\mathbf{e}_h||| + \nu h^2\|\mathbf{u}\|_2^2 + h^2\|\mathbf{u}\|_2\|p\|_1\right).
$$

We also apply the Young's inequality with a positive constant κ satisfying $\kappa < 1/C$,

$$
\begin{aligned}
&\nu h\|\mathbf{u}\|_2|||\mathbf{e}_h||| \le \nu\left(\frac{h^2}{2\kappa}\|\mathbf{u}\|_2^2 + \frac{\kappa}{2}|||\mathbf{e}_h|||^2\right), \\
&h\|p\|_1|||\mathbf{e}_h||| \le \left(\frac{h^2}{2\nu\kappa}\|p\|_1^2 + \frac{\nu\kappa}{2}|||\mathbf{e}_h|||^2\right), \\
&h^2\|\mathbf{u}\|_2\|p\|_1 \le \left(\frac{\nu h^2}{2}\|\mathbf{u}\|_2^2 + \frac{h^2}{2\nu}\|p\|_1^2\right).
\end{aligned}
$$

We finally obtain

$$
\nu|||\mathbf{e}_h|||^2 \le C\left(\nu h^2\|\mathbf{u}\|_2^2 + \frac{h^2}{\nu}\|p\|_1^2\right),
$$

which implies that

$$
|||\mathbf{e}_h||| \le Ch\left(\|\mathbf{u}\|_2 + \frac{1}{\nu}\|p\|_1\right).
$$

In addition, together with this velocity error estimate, the estimate (4.12) implies

$$
\|\epsilon_h\|_0 \le Ch\left(\nu\|\mathbf{u}\|_2 + \|p\|_1\right). \quad \square
$$

Finally, we present the total error estimates showing the optimal rates of convergence in both velocity and pressure.

Theorem 4.9. *Under the same assumption of Theorem 4.8, we have the following error estimates*

$$
\begin{aligned}
&|||\mathbf{u}-\mathbf{u}_h||| \le Ch\left(\|\mathbf{u}\|_2 + \frac{1}{\nu}\|p\|_1\right), \\
&\|p-p_h\|_0 \le Ch\left(\nu\|\mathbf{u}\|_2 + \|p\|_1\right).
\end{aligned}
$$

Proof. The estimates in this theorem are readily proved by the triangle inequality, the interpolation error estimates (4.2b) and (4.7), and the norm equivalence (4.1). $\square$

5. A pressure-robust modified enriched Galerkin method

In this section, we derive a pressure-robust scheme associated with the mEG method (Algorithm 2) by applying the velocity reconstruction operator [31] to the load vector on the right hand side. The operator $\mathcal{R}:\mathbf{V}_h\to\mathcal{BDM}_1(\mathcal{T}_h)\subset H(\mathrm{div},\Omega)$ is defined by

$$
\int_e (\mathcal{R}\mathbf{v})\cdot\mathbf{n}_e p_1\, ds = \int_e \{\mathbf{v}\}\cdot\mathbf{n}_e p_1\, ds, \quad \forall p_1\in P_1(e),\ \forall e\in\mathcal{E}_h^o, \tag{5.1a}
$$

$$
\int_e (\mathcal{R}\mathbf{v})\cdot\mathbf{n}_e p_1\, ds = 0, \qquad \forall p_1\in P_1(e),\ \forall e\in\mathcal{E}_h^b, \tag{5.1b}
$$

when $\mathcal{BDM}_1(\mathcal{T}_h)$ denotes the Brezzi-Douglas-Marini space of index 1 on $\mathcal{T}_h$.

Algorithm 3 Pressure-robust modified enriched Galerkin (PR-mEG) method.

Find $(\mathbf{u}_h,p_h)\in\mathbf{V}_h\times Q_h$ such that

$$
\mathbf{a}_w(\mathbf{u}_h,\mathbf{v}) - \mathbf{b}_w(\mathbf{v},p_h) = (\mathbf{f},\mathcal{R}\mathbf{v})_{\mathcal{T}_h}, \quad \forall\mathbf{v}\in\mathbf{V}_h, \tag{5.2a}
$$

$$
\mathbf{b}_w(\mathbf{u}_h,q) = 0, \qquad \forall q\in Q_h, \tag{5.2b}
$$

where $\mathbf{a}_w(\cdot,\cdot)$ and $\mathbf{b}_w(\cdot,\cdot)$ are the same as (3.6a) and (3.6b), respectively.

Remark 5.1. The mEG method in Algorithm 2 and PR-mEG method in Algorithm 3 have the same formulation on left hand side that consists of $\mathbf{a}_w(\cdot,\cdot)$ and $\mathbf{b}_w(\cdot,\cdot)$. The only difference is that a reconstructed test function is applied to the load vector on the right hand side. This implies that the well-posedness of the PR-mEG method is guaranteed by that of the mEG method, and moreover, both of the mEG and PR-mEG methods produce the same stiffness matrix.

The error equations corresponding to the PR-mEG method are derived in the following lemma using the same error functions in (4.9).

Lemma 5.2. *For any $\mathbf{v} \in \mathbf{V}_h$ and $q \in Q_h$, we have*

$$\mathbf{a}_w(\mathbf{e}_h, \mathbf{v}) - \mathbf{b}_w(\mathbf{v}, \epsilon_h) = l_1(\mathbf{u}, \mathbf{v}) + l_2(\mathbf{u}, \mathbf{v}) + l_3(\mathbf{u}, \mathbf{v}) + \mathbf{s}(\Pi_h \mathbf{u}, \mathbf{v}), \tag{5.3a}$$

$$\mathbf{b}_w(\mathbf{e}_h, q) = -\mathbf{b}_w(\chi_h, q), \tag{5.3b}$$

where $l_1(\cdot,\cdot)$, $l_2(\cdot,\cdot)$, and $\mathbf{s}(\cdot,\cdot)$ are defined in Lemma 4.6, and another supplemental bilinear form is defined by

$$l_3(\mathbf{u}, \mathbf{v}) = -\nu \left(\Delta \mathbf{u}, \mathbf{v} - \mathcal{R}\mathbf{v}\right)_{\mathcal{T}_h}$$

Proof. First of all, we obtain the following identities,

$$(\nabla p, \mathcal{R}\mathbf{v})_{\mathcal{T}_h} = -\mathbf{b}(\mathbf{v}, \mathcal{P}_0 p) = -\mathbf{b}_w(\mathbf{v}, \mathcal{P}_0 p)$$

because $\mathcal{R}\mathbf{v} \cdot \mathbf{n}$ is continuous on ∂T and $\nabla \cdot \mathcal{R}\mathbf{v}$ is constant in T. (See [31] for details.) Moreover, we have

$$(-\Delta \mathbf{u}, \mathcal{R}\mathbf{v})_{\mathcal{T}_h} = (-\Delta \mathbf{u}, \mathbf{v})_{\mathcal{T}_h} + (\Delta \mathbf{u}, \mathbf{v} - \mathcal{R}\mathbf{v})_{\mathcal{T}_h}.$$

Then, it follows from (1.1a) and the error equations in Lemma 4.6 that

$$\mathbf{a}_w(\Pi_h \mathbf{u}, \mathbf{v}) - \mathbf{b}_w(\mathbf{v}, \mathcal{P}_0 p) = (\mathbf{f}, \mathcal{R}\mathbf{v})_{\mathcal{T}_h} + l_1(\mathbf{u}, \mathbf{v}) + l_2(\mathbf{u}, \mathbf{v}) + l_3(\mathbf{u}, \mathbf{v}) + \mathbf{s}(\Pi_h \mathbf{u}, \mathbf{v}).$$

By subtracting (5.2a) from this equation, we arrive at the equation (5.3a). The equation (5.3b) is simply derived in the same way as Lemma 4.6. □

Consequently, the following theorem theoretically shows pressure robustness of the PR-mEG method.

Theorem 5.3. *Let $(\mathbf{u}, p) \in [H_0^1(\Omega) \cap H^2(\Omega)]^d \times (L_0^2(\Omega) \cap H^1(\Omega))$ be the solution to (1.1a)-(1.1c), and $(\mathbf{u}_h, p_h) \in \mathbf{V}_h \times Q_h$ be the discrete solution from the PR-mEG method. Then, we have the following error estimates*

$$|||\Pi_h \mathbf{u} - \mathbf{u}_h||| \le Ch\|\mathbf{u}\|_2, \quad \|\mathcal{P}_0 p - p_h\|_0 \le C\nu h\|\mathbf{u}\|_2.$$

Therefore, the total error estimates are as follows:

$$|||\mathbf{u} - \mathbf{u}_h||| \le Ch\|\mathbf{u}\|_2, \quad \|p - p_h\|_0 \le Ch\left(\nu\|\mathbf{u}\|_2 + \|p\|_1\right).$$

Proof. To begin with, we observe the error equation (5.3a),

$$\mathbf{b}_w(\mathbf{v}, \epsilon_h) = \mathbf{a}_w(\mathbf{e}_h, \mathbf{v}) - l_1(\mathbf{u}, \mathbf{v}) - l_2(\mathbf{u}, \mathbf{v}) - l_3(\mathbf{u}, \mathbf{v}) - \mathbf{s}(\Pi_h \mathbf{u}, \mathbf{v}).$$

Here, the bilinear form $l_3(\mathbf{u}, \mathbf{v})$ is bounded using the Cauchy-Schwarz inequality,

$$|l_3(\mathbf{u}, \mathbf{v})| \le \nu\|\Delta \mathbf{u}\|_0 \|\mathbf{v} - \mathcal{R}\mathbf{v}\|_0 \le \nu\|\mathbf{u}\|_2 \|\mathbf{v} - \mathcal{R}\mathbf{v}\|_0.$$

It also follows from the estimate $\|\mathbf{v} - \mathcal{R}\mathbf{v}\|_0$ in [31] and the norm equivalence (4.1) that

$$\|\mathbf{v} - \mathcal{R}\mathbf{v}\|_0 \le Ch|||\mathbf{v}|||,$$

so we arrive at

$$|l_3(\mathbf{u}, \mathbf{v})| \le C\nu h\|\mathbf{u}\|_2 |||\mathbf{v}|||. \tag{5.4}$$

Thus, from (4.6), (4.11), and (5.4), we obtain

$$|\mathbf{b}_w(\mathbf{v}, \epsilon_h)| \le C\left(\nu|||\mathbf{e}_h||| + \nu h\|\mathbf{u}\|_2\right)|||\mathbf{v}|||.$$

Hence, the inf-sup condition (4.3) leads to

$$\|\epsilon_h\|_0 \le C\nu\left(|||\mathbf{e}_h||| + h\|\mathbf{u}\|_2\right). \tag{5.5}$$

Similar to the proof of Theorem 4.8, choosing $\mathbf{v} = \mathbf{e}_h$ and $q = \epsilon_h$ yields that

$$\mathbf{a}_w(\mathbf{e}_h, \mathbf{e}_h) = -\mathbf{b}_w(\chi_h, \epsilon_h) + l_1(\mathbf{u}, \mathbf{e}_h) + l_2(\mathbf{u}, \mathbf{e}_h) + l_3(\mathbf{u}, \mathbf{e}_h) + \mathbf{s}(\Pi_h \mathbf{u}, \mathbf{e}_h).$$

From (4.13) and (5.5), we get the following intermediate result,

$$|\mathbf{b}_w(\chi_h, \epsilon_h)| \le Ch\|\mathbf{u}\|_2 \|\epsilon_h\|_0 \le C\nu h\|\mathbf{u}\|_2 \left(|||\mathbf{e}_h||| + h\|\mathbf{u}\|_2\right).$$

Therefore, it follows from (4.5), (4.11), and (5.4) that

$$\nu|||\mathbf{e}_h|||^2 \le C\nu\left(h\|\mathbf{u}\|_2|||\mathbf{e}_h||| + h^2\|\mathbf{u}\|_2^2\right).$$

The Young's inequality gives

$$h\|\mathbf{u}\|_2|||\mathbf{e}_h||| \le \frac{h^2}{2\kappa}\|\mathbf{u}\|_2^2 + \frac{\kappa}{2}|||\mathbf{e}_h|||^2,$$

so choosing a proper κ implies

$$\nu|||\mathbf{e}_h|||^2 \le C\nu h^2\|\mathbf{u}\|_2^2.$$

Therefore, together with (5.5), we obtain

$$|||\mathbf{e}_h||| \le Ch\|\mathbf{u}\|_2, \quad \|\epsilon_h\|_0 \le C\nu h\|\mathbf{u}\|_2. \quad \square$$

6. Numerical experiments

In this section, we present numerical experiments validating our theoretical results with two- and three-dimensional examples. The numerical experiments are implemented by authors' codes developed based on iFEM [35]. The numerical methods mentioned in this paper and their discrete solutions are denoted as follows:

- $(\mathbf{u}_h^{\mathrm{EG}}, p_h^{\mathrm{EG}})$: Solution by the EG method [12] in Algorithm 1.
- $(\mathbf{u}_h^{\mathrm{mEG}}, p_h^{\mathrm{mEG}})$: Solution by the mEG method in Algorithm 2.
- $(\mathbf{u}_h^{\mathrm{PR}}, p_h^{\mathrm{PR}})$: Solution by the PR-mEG method in Algorithm 3.

We compare the penalty terms in the EG and mEG methods,

$$\mathrm{EG}: \text{Penalty term of } \mathbf{a}(\mathbf{u}_h^{\mathrm{EG}}, \mathbf{v}) \quad \to \quad \nu\rho\langle h_e^{-1}[\mathbf{u}_h^{\mathrm{EG}}], [\mathbf{v}]\rangle_{\mathcal{E}_h}, \tag{6.1}$$

$$\mathrm{mEG}: \text{Penalty term of } \mathbf{a}_w(\mathbf{u}_h^{\mathrm{mEG}}, \mathbf{v}) \quad \to \quad \nu\langle h_e^{-1}[\mathbf{u}_h^{\mathrm{mEG}}], [\mathbf{v}]\rangle_{\mathcal{E}_h}. \tag{6.2}$$

While a sufficiently large penalty parameter ρ is required for the EG method with the symmetric formulation, our mEG method is a penalty parameter-free EG method under the same finite-dimensional velocity and pressure spaces. In the numerical results of [12], a non-symmetric formulation has been focused on, which needs a positive penalty parameter $\rho > 0$ for well-posedness. ($\rho = 1$ in the numerical results of [12].) However, our numerical experiments with the symmetric formulation will show the need for a large parameter ρ depending on various factors, especially meshes and example problems.

We recall the error estimates for the mEG method in Section 4:

$$|||\Pi_h \mathbf{u} - \mathbf{u}_h^{\mathrm{mEG}}||| \lesssim h\left(\|\mathbf{u}\|_2 + \nu^{-1}\|p\|_1\right),$$

$$\|\mathcal{P}_0 p - p_h^{\mathrm{mEG}}\|_0 \lesssim h\left(\nu\|\mathbf{u}\|_2 + \|p\|_1\right), \tag{6.3a}$$

$$|||\mathbf{u} - \mathbf{u}_h^{\mathrm{mEG}}||| \lesssim h\left(\|\mathbf{u}\|_2 + \nu^{-1}\|p\|_1\right),$$

$$\|p - p_h^{\mathrm{mEG}}\|_0 \lesssim h\left(\nu\|\mathbf{u}\|_2 + \|p\|_1\right), \tag{6.3b}$$

which means the same rates of convergence as the EG method. Moreover, we developed a pressure-robust numerical scheme corresponding to the mEG method, and the error estimates for the PR-mEG method proved in Section 5 are as follows:

$$|||\Pi_h \mathbf{u} - \mathbf{u}_h^{\mathrm{PR}}||| \lesssim h\|\mathbf{u}\|_2, \quad \|\mathcal{P}_0 p - p_h^{\mathrm{PR}}\|_0 \lesssim \nu h\|\mathbf{u}\|_2, \tag{6.4a}$$

$$|||\mathbf{u} - \mathbf{u}_h^{\mathrm{PR}}||| \lesssim h\|\mathbf{u}\|_2, \quad \|p - p_h^{\mathrm{PR}}\|_0 \lesssim h\left(\nu\|\mathbf{u}\|_2 + \|p\|_1\right). \tag{6.4b}$$

In two- and three-dimensional examples, we demonstrate the well-posedness and optimal rates of convergence for the mEG method. By checking the behaviors of the errors with decreasing viscosity ν, we confirm the error estimates of the PR-mEG method in (6.4), which means

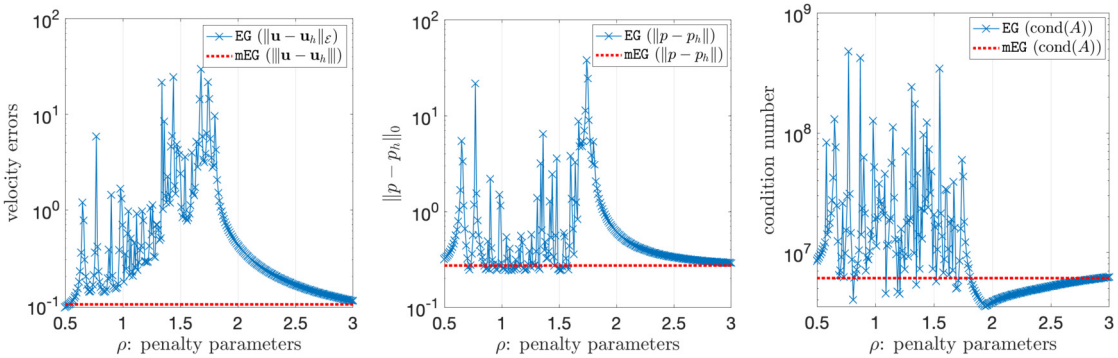

Fig. 1. Errors and condition numbers of mEG and EG for $0.5 \le \rho \le 3$ ($\nu = 1$, $h = 1/16$).

Table 1
A mesh refinement study for EG and mEG with varying mesh size h and $\nu = 1$.

	EG ($\rho = 1$)		EG ($\rho = 3$)		mEG	
h	$\|\mathbf{u}-\mathbf{u}_h^{\mathrm{EG}}\|_\varepsilon$	Order	$\|\mathbf{u}-\mathbf{u}_h^{\mathrm{EG}}\|_\varepsilon$	Order	$\|\|\|\mathbf{u}-\mathbf{u}_h^{\mathrm{mEG}}\|\|\|$	Order
1/8	7.394e-1	-	3.099e-1	-	2.749e-1	-
1/16	6.931e-1	0.09	1.117e-1	1.47	1.024e-1	1.42
1/32	2.440e-1	1.51	4.185e-2	1.42	3.940e-2	1.38
1/64	9.052e-2	1.43	1.670e-2	1.33	1.606e-2	1.29
h	$\|p-p_h^{\mathrm{EG}}\|_0$	Order	$\|p-p_h^{\mathrm{EG}}\|_0$	Order	$\|p-p_h^{\mathrm{mEG}}\|_0$	Order
1/8	9.299e-1	-	6.269e-1	-	5.815e-1	-
1/16	2.897e-1	1.68	2.917e-1	1.10	2.733e-1	1.09
1/32	2.319e-1	0.32	1.402e-1	1.06	1.322e-1	1.05
1/64	2.664e-1	-0.20	6.869e-2	1.03	6.498e-2	1.02

more accurate numerical solutions than the mEG method in the case of small viscosity $\nu \ll 1$.

6.1. Two dimensional tests

Let the computational domain be $\Omega = (0,1)\times(0,1)$. The velocity field and pressure are chosen as

$$\mathbf{u} = \begin{pmatrix} 10x^2(x-1)^2y(y-1)(2y-1) \\ -10x(x-1)(2x-1)y^2(y-1)^2 \end{pmatrix}, \quad p = 10(2x-1)(2y-1). \tag{6.5}$$

Then, the body force $\mathbf{f}$ is obtained from the Stokes equations in (1.1).

6.1.1. Penalty parameter-free test

Homogeneous Dirichlet boundary condition. We consider the example velocity and pressure in (6.5) with the homogeneous Dirichlet boundary condition for velocity. We check the errors and condition numbers of the stiffness matrices to compare the mEG method with the EG method with different penalty parameters. To see how the penalty parameters affect the performance of the EG method, we apply the penalty term (6.1) and change ρ from 0.1 to 3. In this test, we choose the uniform triangular mesh with $h = 1/16$ and the viscosity $\nu = 1$. Fig. 1 shows that the EG method seems to yield unstable errors and condition numbers with penalty parameters less than 2, implying the need of a sufficiently large parameter for stability. On the other hand, the mEG method shows relatively stable errors and condition numbers with the parameter-free penalty term (6.2).

We also perform a mesh refinement study for the mEG method and the EG method with $\rho = 1, 3$. In Table 1, the errors of the EG method fail to converge due to the insufficiently large penalty parameter ($\rho = 1$). When a sufficiently large parameter is applied ($\rho = 3$), the EG method yields the first-order convergence. However, the mEG method produces the velocity and pressure errors that indicate at least the first-order convergence, and those errors are smaller than the EG method's errors.

Moreover, we compare the numerical velocity and pressure of the EG and mEG methods to see how small parameters affect numerical solutions. In Fig. 2, the numerical velocity of the EG method roughly captures the vortex flow pattern, but some relatively large jumps appear throughout the numerical velocity solution. However, the mEG method produces a more stable numerical velocity that captures the pattern better than the EG method.

Mixed boundary conditions. We consider the same example functions (6.5) and mixed boundary conditions on the domain Ω described in Fig. 3,

$$\mathbf{u} = \mathbf{0} \quad \text{on } \Gamma_D,$$
$$(\nu\nabla\mathbf{u} - p\mathbf{I})\mathbf{n} = \mathbf{s} \quad \text{on } \Gamma_N,$$

where $\mathbf{I}$ is the identity tensor on $\mathbb{R}^d$. To implement the boundary conditions, we see that the EG velocity in (3.5) satisfies $\mathbf{u}_h = \mathbf{u}_h^C + \mathbf{u}_h^D = \mathbf{0}$ on any $e \subset \Gamma_D$. Thus, when $\partial T \cap \Gamma_D \neq \emptyset$, the weak gradient for $\mathbf{u}_h^D$ is computed as $\nabla_w \mathbf{u}_h^D\big|_T \in [P_0(T)]^{d\times d}$ such that

$$(\nabla_w \mathbf{u}_h^D, \aleph)_T = \sum_{e\subset\partial T\setminus\Gamma_D} \langle \{\mathbf{u}_h^D\}, \aleph\cdot\mathbf{n}\rangle_e, \quad \forall \aleph \in [P_0(T)]^{d\times d} \tag{6.6}$$

while applying $\mathbf{u}_h^D = \mathbf{0}$ weakly. On the boundary Γ_N, the weak gradient for $\mathbf{u}_h^D$ is obtained using the same manner in Definition 3.1. The boundary condition on Γ_N changes the right hand side in (3.5a) to $(\mathbf{f},\mathbf{v}) + \langle \mathbf{s},\mathbf{v}\rangle_{\Gamma_N}$.

Fig. 3 compares the errors of mEG and EG methods and shows a mesh refinement study for the mEG method with the mixed boundary conditions. The error comparison implies that the EG method requires a large penalty parameter to provide the desired accuracy. On the other hand, we confirm from Fig. 3 that the mEG method yields relatively smaller errors and guarantees first-order convergence without such a parameter.

Various meshes. We also conduct the penalty parameter-free test on various meshes presented in Fig. 4:

- `Perturbed mesh`: The uniform triangular mesh is randomly perturbed, so some very sharp triangles are generated. The velocity field and pressure in (6.5) are considered. The homogeneous boundary condition is applied.
- `Square with hole`: The computational domain is the unit square with a hole in the middle. An adaptive mesh is generated with triangles of different sizes to capture the circle in the middle. The velocity field and pressure in (6.5) are considered. The homogeneous boundary condition is applied on the outer square, but a non-homogeneous Dirichlet boundary condition occurs on the circle. For a non-homogeneous Dirichlet boundary condition ($\mathbf{u} = \mathbf{g}$ on $\partial\Omega$), the EG velocity satisfies $\mathbf{u}_h = \mathbf{u}_h^C + \mathbf{u}_h^D = \mathbf{g}$ on any $e \subset \partial\Omega$. We impose $\mathbf{u}_h^C = \mathbf{g}$ strongly, while applying $\mathbf{u}_h^D = \mathbf{0}$ weakly as introduced in (6.6).
- `L-shape`: The computational domain is the L-shaped domain. The velocity field and pressure are chosen as

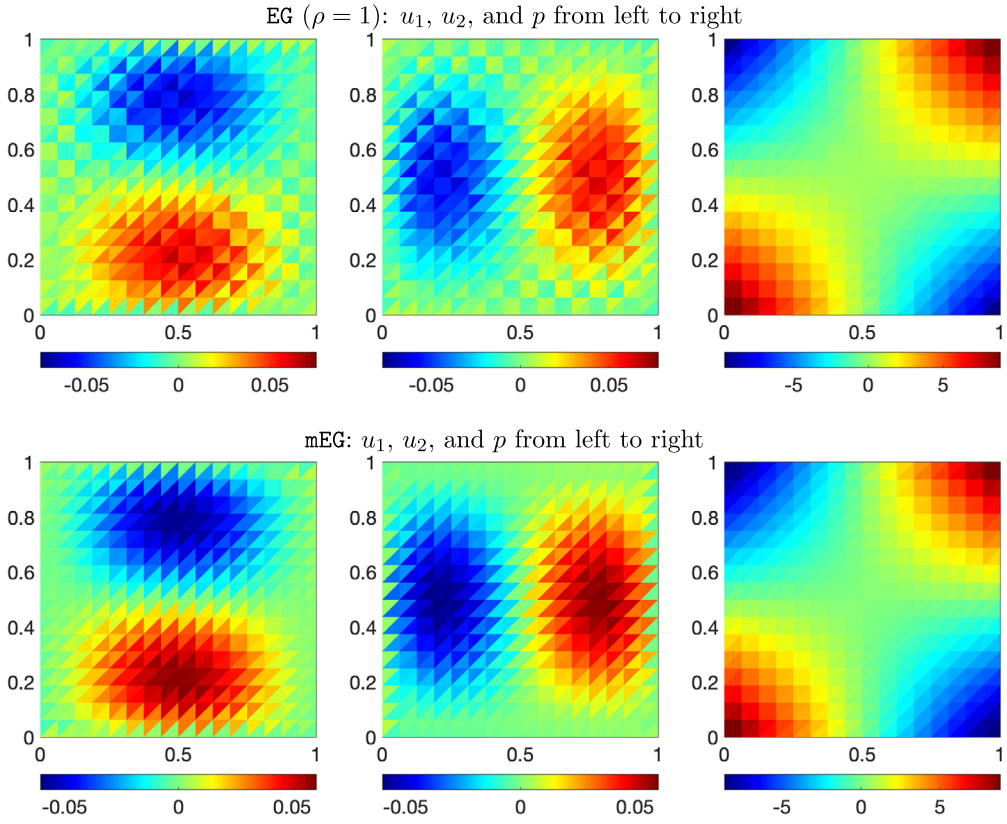

Fig. 2. Comparison of the numerical solutions with $h = 1/16$ and $\nu = 1$.

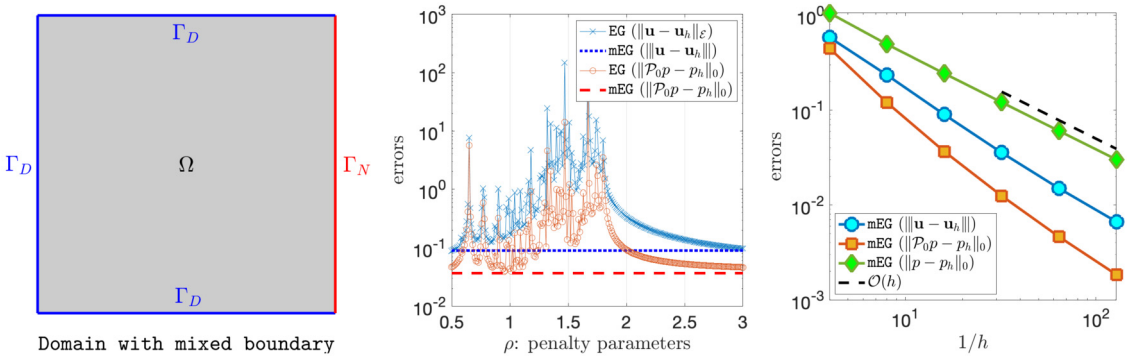

Fig. 3. The unit square domain with mixed boundary conditions (left), comparison of the mEG and EG methods' errors for $\nu = 1$ and $h = 1/16$ (middle), and a mesh refinement study for mEG with $\nu = 1$ (right).

$\mathbf{u}(x, y) = (\sin(\pi x)\sin(\pi y), \cos(\pi x)\cos(\pi y))$ and $p(x, y) = (x^2 + y^2)^{-1/3}$.

Due to the singularity of the pressure at the center, an adaptive mesh is generated with triangles of the same shape.

Fig. 4 shows the above meshes, the corresponding mesh qualities, and the errors of the EG and mEG methods. The mesh quality of a triangle [36] is defined as the ratio of its area to the sum of the squares of its sides, which implies that the equilateral triangle has the best mesh quality 1 and sharper triangles are closer to 0. The EG method still requires large penalty parameters to achieve stable errors. Moreover, such large parameters depend on the meshes. Specifically, in the Perturbed mesh, some bad-quality triangles cause an unexpected spike around $\rho = 3$ in the velocity errors, making choosing a proper penalty parameter more difficult. In the L-shape with an adaptive mesh, the EG method's pressure error tends to increase as ρ gets larger after a minimum occurs. However, regardless of a penalty parameter, the mEG method seems uniformly stable on all the given meshes. The mEG method, even for a mesh with bad-quality triangles and adaptive meshes, has good performance. These numerical results confirm that the mEG method is a penalty parameter-free scheme.

6.1.2. *Pressure-robust test*

In this test, we verify the pressure robustness of the PR-mEG method. We solve the example problem (6.5) with varying ν, from 10^{-1} to 10^{-6}, to confirm the error behaviors expected in (6.3) and (6.4). The mesh size is fixed as $h = 1/32$. Fig. 5 shows the velocity errors $|||\mathbf{u} - \mathbf{u}_h|||$ and pressure errors $\|\mathcal{P}_0 p - p_h\|_0$ of the mEG and PR-mEG methods. In Fig. 5, the mEG method produces the velocity errors proportional to ν^{-1} because the second term $h\nu^{-1}\|p\|_1$ of the error bound (6.3b) becomes dominant as ν gets smaller. Also, since the pressure error $\|\mathcal{P}_0 p - p_h^{\text{mEG}}\|_0$ is bounded by a dominant term $h\|p\|_1$, the error remains the same. On the other hand, the PR-mEG method produces the same velocity errors regardless of ν, and its pressure errors decrease in proportion to ν. These

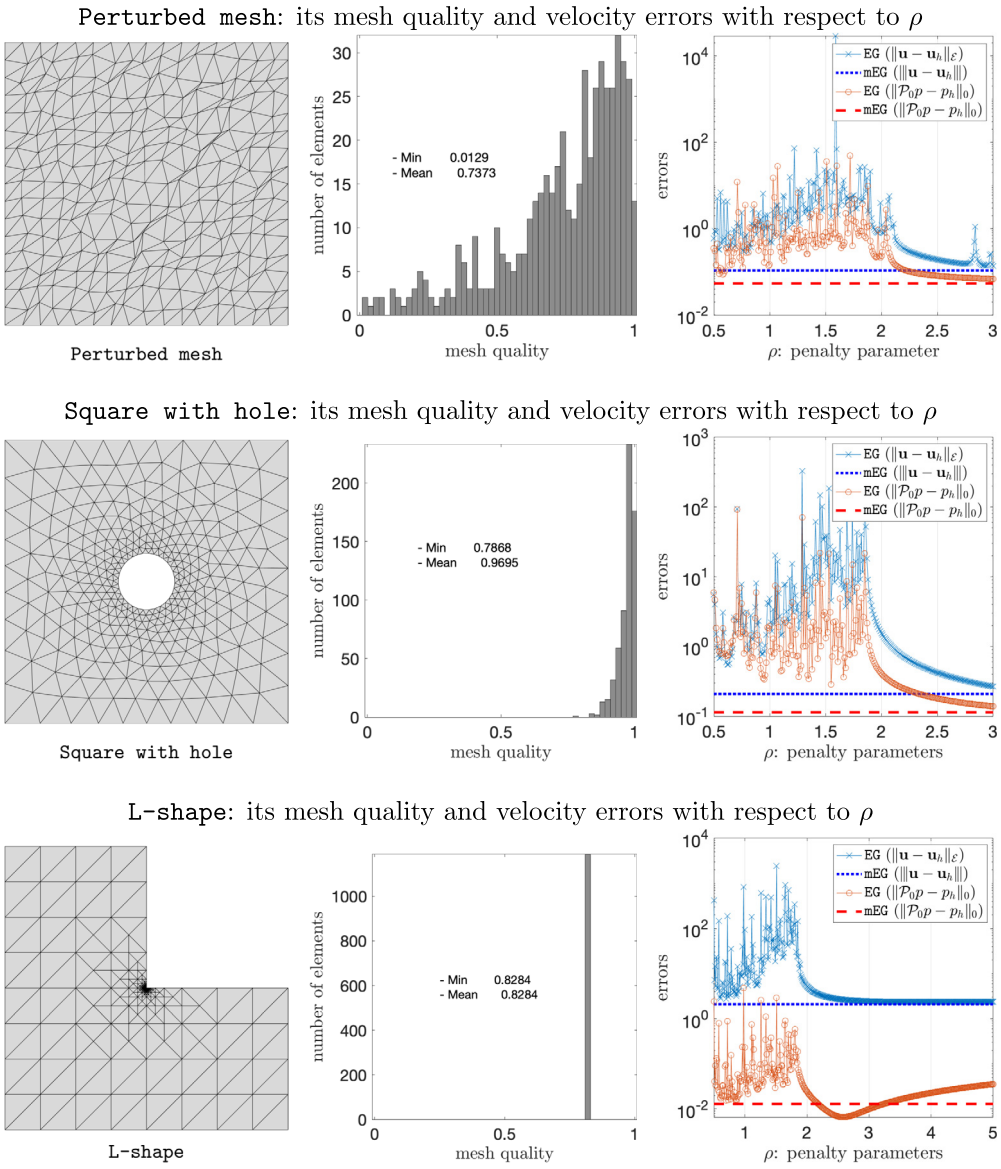

Fig. 4. Comparison of EG and mEG on various meshes ($\nu = 1$).

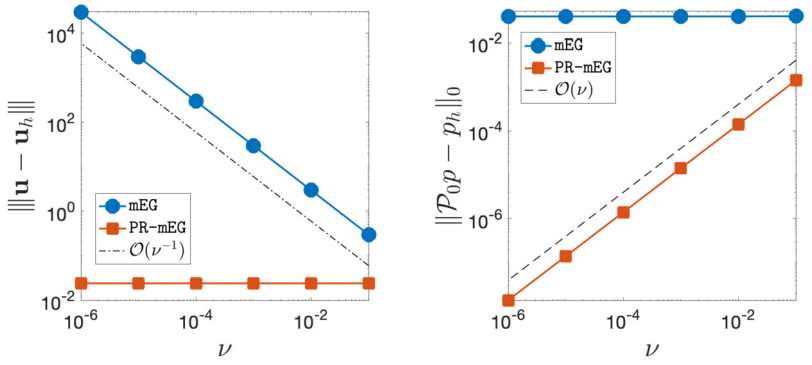

Fig. 5. Error profiles of the mEG and PR-mEG methods with varying ν values and a fixed mesh size $h = 1/32$.

numerical results support our theoretical error estimates related to the pressure robustness in (6.3) and (6.4).

Furthermore, we perform a mesh refinement study for the mEG and PR-mEG methods with decreasing mesh size h and fixed $\nu = 10^{-6}$. As shown in Table 2, both methods' velocity and pressure errors decrease in at least the first order of convergence, and the pressure errors look very similar in magnitude. However, even though the velocity errors for the mEG method decrease faster, the magnitude of the errors seems enormous. Thus, obtaining accurate numerical velocity from the mEG method may not be possible unless h is small enough. On the other

Table 2
A mesh refinement study for mEG and PR-mEG with varying mesh size h and $\nu = 10^{-6}$.

	mEG		PR-mEG	
h	$\|\|\|\mathbf{u}-\mathbf{u}_h^{\mathrm{mEG}}\|\|\|$	Order	$\|\|\|\mathbf{u}-\mathbf{u}_h^{\mathrm{PR}}\|\|\|$	Order
1/8	2.577e+5	-	9.727e-2	-
1/16	9.097e+4	1.50	4.749e-2	1.03
1/32	3.183e+4	1.52	2.339e-2	1.02
1/64	1.116e+4	1.51	1.159e-2	1.01
h	$\|p-p_h^{\mathrm{mEG}}\|_0$	Order	$\|p-p_h^{\mathrm{PR}}\|_0$	Order
1/8	5.736e-1	-	4.802e-1	-
1/16	2.694e-1	1.09	2.404e-1	1.00
1/32	1.310e-1	1.04	1.203e-1	1.00
1/64	6.464e-2	1.02	6.014e-2	1.00

Table 3
Each term computed in EG and mEG and the numbers of calculations with $h = 1/70$ (m: million).

EG	$\mathbf{a}(\mathbf{w},\mathbf{v})$	# of cals	$\mathbf{b}(\mathbf{w},\mathbf{v})$	# of cals
$\mathcal{T}_h$-terms	$(\nabla\mathbf{w},\nabla\mathbf{v})_{\mathcal{T}_h}$	150 m	$(\nabla\cdot\mathbf{w},q)_{\mathcal{T}_h}$	54 m
$\mathcal{E}_h$-terms	$\langle\{\nabla\mathbf{w}\}\cdot\mathbf{n}_e,[\mathbf{v}]\rangle_{\mathcal{E}_h}$	431 m	$\langle[\mathbf{w}]\cdot\mathbf{n}_e,\{q\}\rangle_{\mathcal{E}_h}$	33 m
Penalty term	$\rho\langle h_e^{-1}[\mathbf{w}],[\mathbf{v}]\rangle_{\mathcal{E}_h}$	17 m	-	-
mEG	$\mathbf{a}_w(\mathbf{w},\mathbf{v})$	# of cals	$\mathbf{b}_w(\mathbf{w},\mathbf{v})$	# of cals
Weak derivatives	$\nabla_w\mathbf{v}$	10 m	$\nabla_w\cdot\mathbf{v}$	10 m
$\mathcal{T}_h$-terms	$(\nabla_w\mathbf{w},\nabla_w\mathbf{v})_{\mathcal{T}_h}$	397 m	$(\nabla_w\cdot\mathbf{w},q)_{\mathcal{T}_h}$	70 m
Penalty term	$\langle h_e^{-1}[\mathbf{w}],[\mathbf{v}]\rangle_{\mathcal{E}_h}$	17 m	-	-

hand, the PR-mEG method yields about a million times smaller velocity errors than the mEG method, which means that the PR-mEG method provides a significantly improved numerical velocity for the Stokes equations with small viscosity.

6.2. Three dimensional tests

We consider a 3D flow in a unit cube $\Omega = (0,1)^3$. The velocity field and pressure are chosen as

$$\mathbf{u} = \begin{pmatrix} \sin(\pi x)\cos(\pi y) - \sin(\pi x)\cos(\pi z) \\ \sin(\pi y)\cos(\pi z) - \sin(\pi y)\cos(\pi x) \\ \sin(\pi z)\cos(\pi x) - \sin(\pi z)\cos(\pi y) \end{pmatrix}, \quad p = \sin(\pi x)\sin(\pi y)\sin(\pi z). \tag{6.7}$$

6.2.1. Low-cost test

In this 3D example, we compare the computational cost of the EG and mEG methods. Table 3 displays each term that needs to be computed in the two methods. In the EG method, we divide the bilinear forms into three parts, $\mathcal{T}_h$-terms, $\mathcal{E}_h$-terms, and penalty terms. Table 3 also shows how many calculations are involved when assembling the stiffness matrix with $h = 1/70$. For example, with $\mathbf{v} = \mathbf{v}^C + \mathbf{v}^D$ implying $[\mathbf{v}^C] = 0$ and $[\mathbf{v}^D] \neq 0$ on each $e \in \mathcal{E}_h$, the penalty term is calculated as

$$\rho\langle h_e^{-1}[\mathbf{w}^D],[\mathbf{v}^D]\rangle_{\mathcal{E}_h} = \rho\langle h_e^{-1}[\mathbf{x}-\mathbf{x}_{T^\pm}],[\mathbf{x}-\mathbf{x}_{T^\pm}]\rangle_{\mathcal{E}_h}$$

when $e \in \partial T^+ \cap \partial T^-$ for each $e \in \mathcal{E}_h$, yielding approximately $(2\times 2)|\mathcal{E}_h| \approx 17$ million calculations. Many calculations are generated if $\mathbf{v}^C$ is involved in assembling the stiffness matrix, such as $(\nabla\mathbf{w}^C,\nabla\mathbf{v}^C)_{\mathcal{T}_h}$ and $\langle\{\nabla\mathbf{w}^C\}\cdot\mathbf{n}_e,[\mathbf{v}^D]\rangle_{\mathcal{E}_h}$. This is because there are four barycentric coordinates for each component of $\mathbf{v}^C$ in $T \in \mathcal{T}_h$. On the other hand, in the initial step of implementing the mEG method, a small amount of computational cost is required to compute the weak gradient $\nabla_w\mathbf{v}^D$. From Remark 3.2, we recall the weak gradient $\nabla_w\mathbf{v}^D$ locally determined by

$$(\nabla_w\mathbf{v}^D)_{i,j} = \frac{n_j}{|T|}\langle\{\mathbf{v}^D\},\mathbf{e}_i\rangle_{\partial T}, \quad 1\le i,j\le 3,$$

Table 4
A mesh refinement study for EG and mEG with varying mesh size h and $\nu = 1$ in the 3D case.

	EG ($\rho=2$)		EG ($\rho=10$)		mEG	
h	$\|\|\mathbf{u}-\mathbf{u}_h^{\mathrm{EG}}\|\|_{\mathcal{E}}$	Order	$\|\|\mathbf{u}-\mathbf{u}_h^{\mathrm{EG}}\|\|_{\mathcal{E}}$	Order	$\|\|\|\mathbf{u}-\mathbf{u}_h^{\mathrm{mEG}}\|\|\|$	Order
1/4	2.518e+0	-	3.719e+0	-	2.284e+0	-
1/8	1.228e+0	1.04	1.827e+0	1.03	1.121e+0	1.03
1/16	6.052e-1	1.02	9.048e-1	1.01	5.552e-1	1.01
1/32	3.007e-1	1.01	4.501e-1	1.01	2.764e-1	1.01
h	$\|p-p_h^{\mathrm{EG}}\|_0$	Order	$\|p-p_h^{\mathrm{EG}}\|_0$	Order	$\|p-p_h^{\mathrm{mEG}}\|_0$	Order
1/4	8.819e-1	-	8.377e+0	-	1.349e+0	-
1/8	3.611e-1	1.29	3.600e+0	1.22	6.098e-1	1.15
1/16	1.688e-1	1.10	1.670e+0	1.11	3.011e-1	1.02
1/32	8.411e-2	1.00	8.312e-1	1.01	1.504e-1	1.00

where n_j is the j-th component of $\mathbf{n}$ and $\mathbf{e}_i$ is the standard unit vector whose i-th component is 1. The surface integral is calculated by the one-point quadrature rule on each face because $\mathbf{v}^D|_T$ is a linear vector function. Since each $T \in \mathcal{T}_h$ has four adjacent elements, five basis functions of $\mathbf{v}^D$ (in T and adjacent elements) imply a nonzero weak gradient in each T. Thus, as shown in Table 3, $(\nabla_w\mathbf{w},\nabla_w\mathbf{v})$ yields more calculations than $(\nabla\mathbf{w},\nabla\mathbf{v})$.

Fig. 6 shows the comparison of $|\mathcal{T}_h|$ and $|\mathcal{E}_h|$, the numbers of calculations, and the elapsed time to assemble the stiffness matrix. Since $|\mathcal{E}_h|$ is almost twice as many as $|\mathcal{T}_h|$ and the EG method requires a lot of calculations on $e \in \mathcal{E}_h$, the total number of calculations in the EG method is larger than that in mEG method. When assembling the stiffness matrix, we use the vectorization technique introduced in iFEM [35] and a MATLAB built-in function 'sparse' [37] to avoid large for loops (see [38] for details). The function 'sparse' uses inputs i, j, and v, where i is the information of rows, j is the information of columns, and v consists of the components of a matrix. Most of the elapsed time is spent calling the function 'sparse', and the computational cost of 'sparse' depends on the number of calculations, i.e. the size of i. Thus, in Fig. 6, we see the similarity between the number of calculations and the elapsed time. In Fig. 6, the graph of the elapsed time shows that the computational cost in computing weak derivatives is low. Also, it requires a lower computational cost to assemble the stiffness matrix of the mEG method. On the other hand, the computation of the $\mathcal{E}_h$-terms tends to require more time than $\mathcal{T}_h$-terms because the jump and average on the boundary are treated separately. For this reason, we conclude that the mEG method has an advantage in assembling the stiffness matrix of the Stokes equations compared to the EG method.

6.2.2. Penalty parameter-free test

We compute the velocity and pressure errors and condition numbers in the EG method with different penalty parameters and compare them with the mEG method's results. Fig. 7 clearly shows the need for a large penalty parameter for the EG method and the dependency of its errors on the parameters. On the other hand, the mEG method produces stable errors and condition numbers without such a large parameter. For comparison, we display velocity error plots and velocity errors of the EG ($\rho = 1, 2$) and mEG methods in Fig. 8. The EG method with $\rho = 1$ yields non-negligible velocity errors over the whole domain, but a large penalty parameter $\rho = 2$ stabilizes such errors, implying a reliable numerical velocity solution. On the other hand, the mEG method's velocity error profile looks better than the EG method without tuning a penalty parameter.

In addition, we focus on the effect of large penalty parameters on the errors and condition numbers. In Fig. 7, the condition numbers of the EG method tend to increase with the parameters ρ, which causes increased velocity and pressure errors. To perform a quantitative comparison, we choose $\rho = 10$ and $\rho = 2$ based on the results in Fig. 7 and report the pressure and velocity errors of the two cases in Table 4. The pressure errors of the EG method with $\rho = 10$ are ten times bigger than

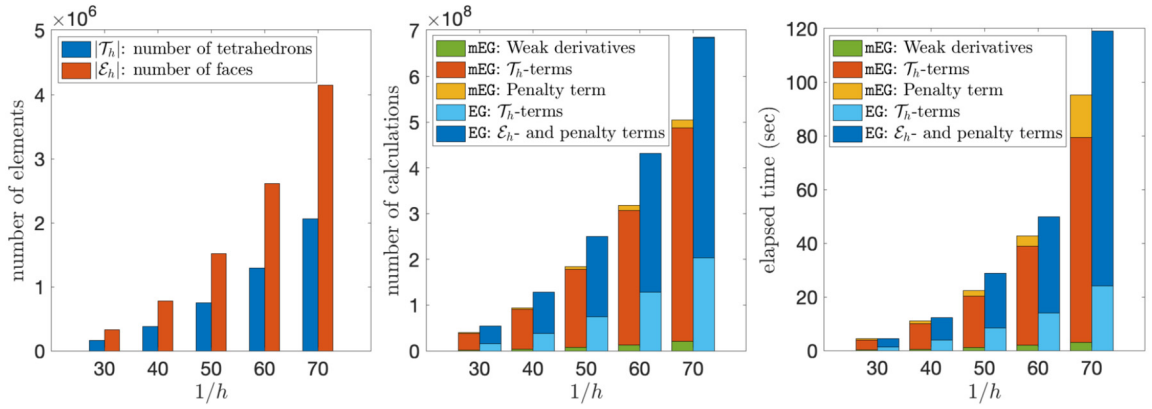

Fig. 6. Comparison of $|\mathcal{T}_h|$ and $|\mathcal{E}_h|$ (left), the number of calculations involved in assembling the stiffness matrix (middle), and the elapsed time to assemble the stiffness matrix (right).

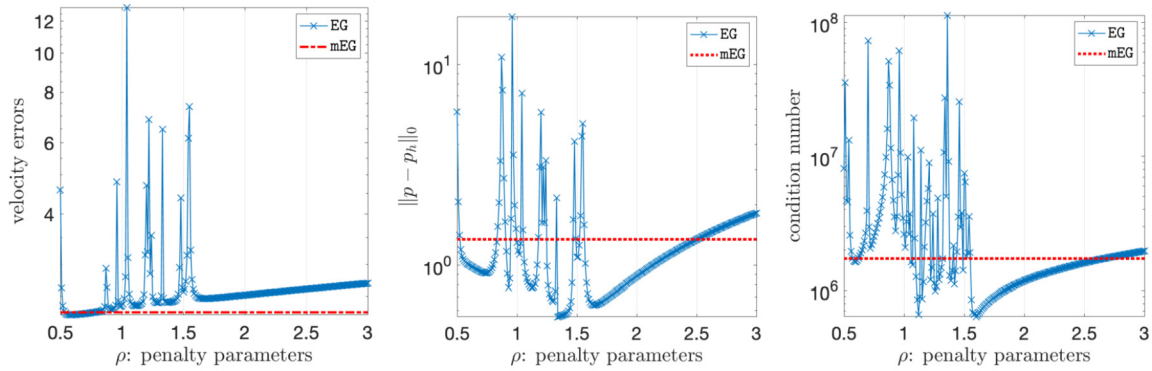

Fig. 7. Errors and condition numbers of mEG and EG for $0.5 \le \rho \le 3$ ($\nu = 1$, $h = 1/4$) in the 3D case.

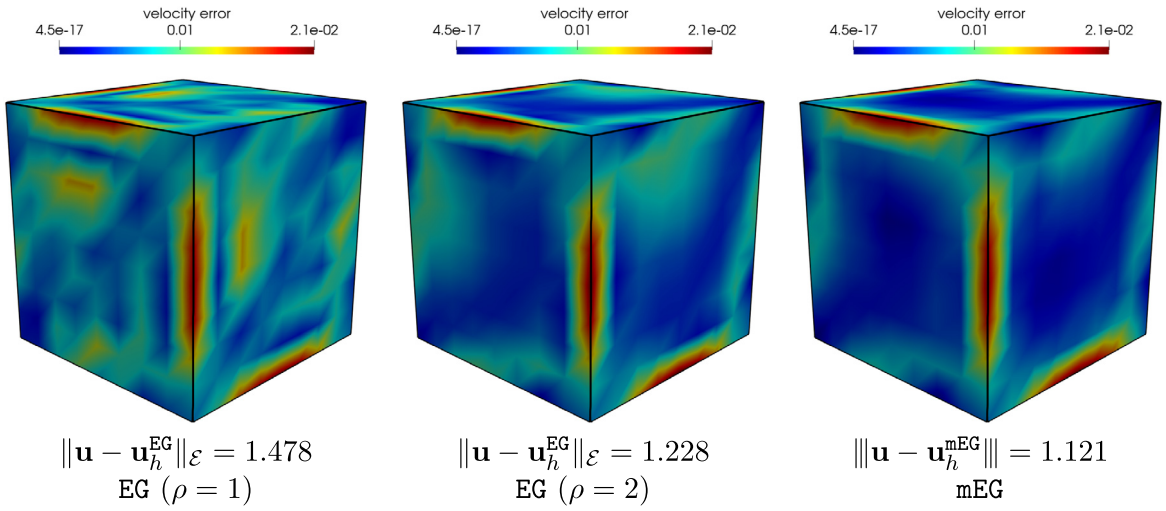

Fig. 8. Velocity error plots and velocity errors of EG and mEG when $h = 1/8$ and $\nu = 1$.

those with $\rho = 2$, even though their pressure errors decrease in the same order. Thus, in practice, a penalty parameter ρ cannot be chosen too large due to this accuracy issue. It may also be challenging to select a proper ρ because it varies with meshes. On the other hand, for the mEG method, the convergence orders of the velocity and pressure errors are at least first-order, and the mEG method yields smaller velocity errors than the EG method with $\rho = 2$. Therefore, with the mEG method, we can always achieve reliable performance without tuning a penalty parameter, making the simulation lower-cost.

6.2.3. *Pressure-robust test*

To verify pressure robustness in the three-dimensional example (6.7), we consider the pattern of the error behaviors obtained from the mEG and PR-mEG methods when ν varies with $h = 1/16$. Fig. 9 shows the same error behaviors as those in the two-dimensional pressure-robust test. For the mEG method, the velocity errors are inversely proportional to ν while the pressure errors tend to stay constant. On the other hand, for the PR-mEG method, the velocity errors seem independent of ν, and the pressure errors decrease in proportion to ν.

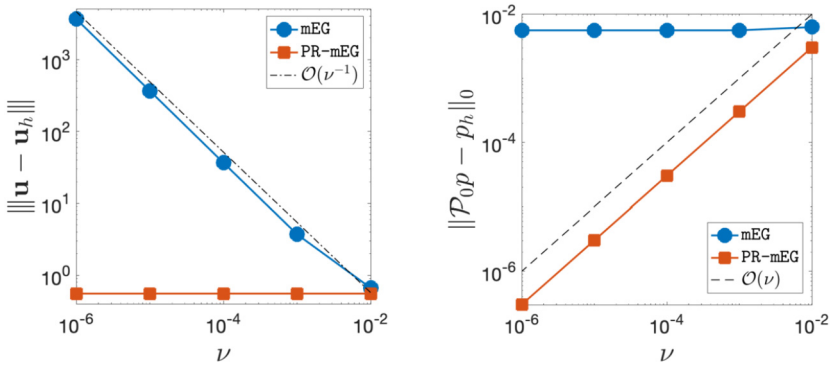

Fig. 9. Error profiles of the mEG and PR-mEG methods with varying ν values and a fixed mesh size $h = 1/16$ in the 3D case.

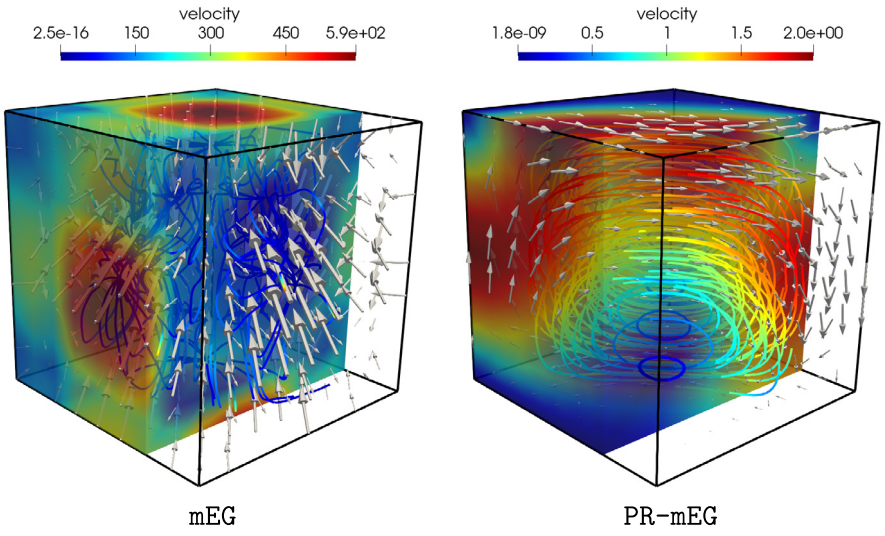

Fig. 10. Streamlines and magnitudes of the 3D numerical velocity when $h = 1/8$ and $\nu = 10^{-6}$.

Furthermore, Fig. 10 shows the streamlines of the numerical velocity solutions of the mEG and PR-mEG methods when $h = 1/8$ and $\nu = 10^{-6}$. In this case, the velocity error of the mEG method is 1.014e+4, while that of the PR-mEG method is 1.122e+0. As shown in Fig. 10, the numerical velocity of the PR-mEG method well captures the 3D vortex flow, while that of the mEG method cannot do so.

7. Conclusion

This paper proposes a low-cost, penalty parameter-free, and pressure-robust Stokes solver based on the EG method operating with minimal degrees of freedom. The weak derivatives, computed by the geometric data of elements, allowed the EG method to be free of penalty parameters and some IPDG trace terms. With reduced computational complexity, the modified EG method preserved the minimal degrees of freedom and the optimal orders of convergence in the EG method. Such features in parameter-free schemes can be used to resolve the computational difficulties in tuning penalty parameters of DG schemes for heterogeneous coefficients, anisotropic problems, moving meshes, and time-dependent problems. Furthermore, the simple modification on the right-hand side achieved pressure robustness for the modified EG method. We also confirmed the improved theoretical results through numerical tests with two- and three-dimensional examples. The idea of using weak derivatives can be applied to enhance other numerical schemes employing the symmetric IPDG formulation. Extending the concept to numerical methods for the biharmonic equation will be one of our future research directions. We expect that the weak derivatives corresponding to the biharmonic equation provide significant computational advantages in numerically solving application problems involving the biharmonic equation.

Data availability

Data will be made available on request.

Acknowledgements

The work of Lin Mu was partially supported by the U.S. National Science Foundation grant DMS-2309557. We would like to thank Prof. Long Chen for his valuable discussions and suggestions on this project.

References

[1] O.A. Ladyzhenskaya, The Mathematical Theory of Viscous Incompressible Flow, vol. 2, Gordon and Breach, New York, 1969.
[2] I. Babuška, The finite element method with Lagrangian multipliers, Numer. Math. 20 (3) (1973) 179–192.
[3] F. Brezzi, On the existence, uniqueness and approximation of saddle-point problems arising from Lagrangian multipliers, Publications mathématiques et informatique de Rennes (S4) (1974) 1–26.
[4] C. Taylor, P. Hood, A numerical solution of the Navier-Stokes equations using the finite element technique, Comput. Fluids 1 (1) (1973) 73–100.
[5] C. Bernardi, G. Raugel, Analysis of some finite elements for the Stokes problem, Math. Comput. 44 (169) (1985) 71–79.
[6] M. Crouzeix, P.-A. Raviart, Conforming and nonconforming finite element methods for solving the stationary Stokes equations I, Revue française d'automatique informatique recherche opérationnelle. Mathématique 7 (R3) (1973) 33–75.

[7] P. Hansbo, M.G. Larson, Piecewise divergence-free discontinuous Galerkin methods for Stokes flow, Commun. Numer. Methods Eng. 24 (5) (2008) 355–366.
[8] V. Girault, B. Rivière, M.F. Wheeler, A discontinuous Galerkin method with nonoverlapping domain decomposition for the Stokes and Navier-Stokes problems, Math. Comput. 74 (249) (2005) 53–84.
[9] J. Wang, X. Ye, A weak Galerkin finite element method for the Stokes equations, Adv. Comput. Math. 42 (1) (2016) 155–174.
[10] L. Mu, J. Wang, X. Ye, S. Zhang, A discrete divergence free weak Galerkin finite element method for the Stokes equations, Appl. Numer. Math. 125 (2018) 172–182.
[11] N. Chaabane, V. Girault, B. Rivière, T. Thompson, A stable enriched Galerkin element for the Stokes problem, Appl. Numer. Math. 132 (2018) 1–21.
[12] S.-Y. Yi, X. Hu, S. Lee, J.H. Adler, An enriched Galerkin method for the Stokes equations, Comput. Math. Appl. 120 (2022) 115–131.
[13] S. Sun, J. Liu, A locally conservative finite element method based on piecewise constant enrichment of the continuous Galerkin method, SIAM J. Sci. Comput. 31 (4) (2009) 2528–2548.
[14] S. Lee, Y.-J. Lee, M.F. Wheeler, A locally conservative enriched Galerkin approximation and efficient solver for elliptic and parabolic problems, SIAM J. Sci. Comput. 38 (3) (2016) A1404–A1429.
[15] S.C. Brenner, L.-Y. Sung, C^0 interior penalty methods for fourth order elliptic boundary value problems on polygonal domains, J. Sci. Comput. 22 (1) (2005) 83–118.
[16] Y. Epshteyn, B. Rivière, Estimation of penalty parameters for symmetric interior penalty Galerkin methods, J. Comput. Appl. Math. 206 (2) (2007) 843–872.
[17] M. Ainsworth, A posteriori error estimation for discontinuous Galerkin finite element approximation, SIAM J. Numer. Anal. 45 (4) (2007) 1777–1798.
[18] M. Ainsworth, R. Rankin, Fully computable error bounds for discontinuous Galerkin finite element approximations on meshes with an arbitrary number of levels of hanging nodes, SIAM J. Numer. Anal. 47 (6) (2010) 4112–4141.
[19] D.A. Di Pietro, A. Ern, Hybrid high-order methods for variable-diffusion problems on general meshes, C. R. Math. 353 (1) (2015) 31–34.
[20] B. Cockburn, J. Gopalakrishnan, R. Lazarov, Unified hybridization of discontinuous Galerkin, mixed, and continuous Galerkin methods for second order elliptic problems, SIAM J. Numer. Anal. 47 (2) (2009) 1319–1365.
[21] J. Wang, X. Ye, A weak Galerkin finite element method for second-order elliptic problems, J. Comput. Appl. Math. 241 (2013) 103–115.
[22] X. Wang, N.S. Malluwawadu, F. Gao, T. McMillan, A modified weak Galerkin finite element method, J. Comput. Appl. Math. 271 (2014) 319–327.
[23] L. Mu, X. Wang, X. Ye, A modified weak Galerkin finite element method for the Stokes equations, J. Comput. Appl. Math. 275 (2015) 79–90.
[24] A. Linke, A divergence-free velocity reconstruction for incompressible flows, C. R. Math. 350 (17–18) (2012) 837–840.
[25] A. Linke, C. Merdon, Pressure-robustness and discrete Helmholtz projectors in mixed finite element methods for the incompressible Navier–Stokes equations, Comput. Methods Appl. Mech. Eng. 311 (2016) 304–326.
[26] N.R. Gauger, A. Linke, P.W. Schroeder, On high-order pressure-robust space discretisations, their advantages for incompressible high Reynolds number generalised Beltrami flows and beyond, SMAI J. Comput. Math. 5 (2019) 89–129.
[27] L. Mu, Pressure robust weak Galerkin finite element methods for Stokes problems, SIAM J. Sci. Comput. 42 (3) (2020) B608–B629.
[28] L. Mu, X. Ye, S. Zhang, Development of pressure-robust discontinuous Galerkin finite element methods for the Stokes problem, J. Sci. Comput. 89 (1) (2021) 1–25.
[29] Y. Li, L.T. Zikatanov, New stabilized $P_1 \times P_0$ finite element methods for nearly inviscid and incompressible flows, Comput. Methods Appl. Mech. Eng. 393 (2022) 114815.
[30] L. Zhao, E.-J. Park, E. Chung, A pressure robust staggered discontinuous Galerkin method for the Stokes equations, Comput. Math. Appl. 128 (2022) 163–179.
[31] X. Hu, S. Lee, L. Mu, S.-Y. Yi, Pressure-robust enriched Galerkin methods for the Stokes equations, arXiv:2208.13076, 2022.
[32] D.A. Di Pietro, A. Ern, Mathematical Aspects of Discontinuous Galerkin Methods, vol. 69, Springer Science & Business Media, 2011.
[33] Y. Xie, S. Cao, L. Chen, L. Zhong, Convergence and optimality of an adaptive modified weak Galerkin finite element method, arXiv:2007.12853, 2020.
[34] S.-Y. Yi, S. Lee, L.T. Zikatanov, Locking-free enriched Galerkin method for linear elasticity, SIAM J. Numer. Anal. 60 (1) (2022) 52–75.
[35] L. Chen, iFEM: an Integrated Finite Element Methods Package in MATLAB, Technical Report, University of California at Irvine, 2009.
[36] L. Chen, Mesh smoothing schemes based on optimal Delaunay triangulations, in: IMR, 2004, pp. 109–120.
[37] J.R. Gilbert, C. Moler, R. Schreiber, Sparse matrices in MATLAB: design and implementation, SIAM J. Matrix Anal. Appl. 13 (1) (1992) 333–356.
[38] L. Chen, Programming of finite element methods in MATLAB, arXiv:1804.05156, 2018.